



# Zircon U–Pb geochronology and heavy mineral composition of the Camaná Formation, southern Peru: Constraints on sediment provenance and uplift of the Coastal and Western Cordilleras



Aldo Alván <sup>a,\*</sup>, Hilmar von Eynatten <sup>a</sup>, István Dunkl <sup>a</sup>, Axel Gerdés <sup>b</sup>

<sup>a</sup> University of Göttingen, Geoscience Center, Department of Sedimentology and Environmental Geology, Goldschmidtstrasse 3, D-37077, Germany

<sup>b</sup> University of Frankfurt, Institute of Geosciences, Altenhofer Allee 1, D-60431, Germany

## ARTICLE INFO

### Article history:

Received 27 August 2014

Accepted 23 February 2015

Available online 13 March 2015

### Keywords:

Provenance analysis

Camaná Formation

U–Pb geochronology

Heavy minerals

Central Andes

Coastal Cordillera

## ABSTRACT

In the forearc of the Central Andes of southern Peru, the Cenozoic Camaná Basin ( $16^{\circ}25'S$  to  $17^{\circ}15'S$ ) forms a ~NW–SE elongated depression filled with coarse-grained deltaic and fluvial deposits. These deposits are termed Camaná Formation. We have applied for the first time, advanced multi-method analytical techniques to sediments of the Camaná Formation in order to define precise sedimentation ages, unravel sediment provenance, and to explain its tectono-sedimentary evolution.

Zircon U–Pb geochronology and multiple geological evidences suggest that the Camaná Formation ranges in age from Late Oligocene to Late Miocene, and may even extend into the Pliocene. We propose a provenance model for the Camaná Formation based on U–Pb geochronology, heavy mineral analysis, and single-grain mineral chemistry by LA-ICP-MS. This model suggests that sediments of the lower part of the Camaná Formation derive from rocks forming the Coastal Cordillera (i.e. the Arequipa Massif and the San Nicolas Batholith) and the widespread ignimbrites of the ~24–10 Ma Huayllillas volcanic arc. In contrast, sediments of the upper part of the Camaná Formation derive predominantly from rocks forming the Western Cordillera (i.e. the Arequipa Massif, the Tacaza Group, and the Coastal Batholith) and products of the ~10–3 Ma Lower Barroso volcanic arc). Accordingly, we infer that uplift of the Coastal Cordillera has strongly influenced deposition of the Camaná Formation since Late Oligocene. A marked shift in provenance within the Camaná Formation at around Middle to Late Miocene time (14–12 Ma) suggests drastic uplift of the Western Cordillera at that time. This uplift has triggered increased relief and erosion in the Western Cordillera, and subsequent deposition of fluvial conglomerates in the Camaná Basin.

© 2015 Elsevier Ltd. All rights reserved.

## 1. Introduction

This manuscript focuses on the derivation of a chronostratigraphically well-defined provenance model for the Cenozoic Camaná Formation that explains consistently the interplay of tectonics and sedimentation in this segment of the southern Peruvian forearc (Fig. 1). Our study relies on shallow-marine coarse-grained deltaic and fluvial deposits. Such deposits mark the interface between terrestrial and marine environments and are generally

considered to intimately reflect uplift and erosion of the basin borders and/or the hinterland (e.g. Colella, 1988; Gawthorpe et al., 1990; Schlunegger et al., 1997; Gawthorpe and Colella, 1990). In the Camaná Basin, such deposits have already been analyzed in terms of sedimentary facies, stratigraphic architecture, and sequence stratigraphy (Alván and von Eynatten, 2014).

Sedimentary provenance analysis refers to the reconstruction of source area geology, the type of source rocks exposed, and the processes that modify the sediment on their way from source to sink (Weltje and von Eynatten, 2004). The compositional characteristics of a sedimentary basin fill are commonly controlled by the lithology of the respective source rock, weathering, erosion, sediment transport processes, and the nature of sedimentary processes within the basin. In many provenance studies emphasis is placed on high density accessory minerals (i.e. heavy minerals) because they

\* Corresponding author. Present address: INGEMMET, Dirección de Geología Regional, Av. Canadá 1470, Lima, Peru.

E-mail addresses: [aalvand@gwdg.de](mailto:aalvand@gwdg.de) (A. Alván), [hilmar.von.eynatten@geo.uni-goettingen.de](mailto:hilmar.von.eynatten@geo.uni-goettingen.de) (H. von Eynatten), [istvan.dunkl@geo.uni-goettingen.de](mailto:istvan.dunkl@geo.uni-goettingen.de) (I. Dunkl), [gerdes@em.uni-frankfurt.de](mailto:gerdes@em.uni-frankfurt.de) (A. Gerdés).

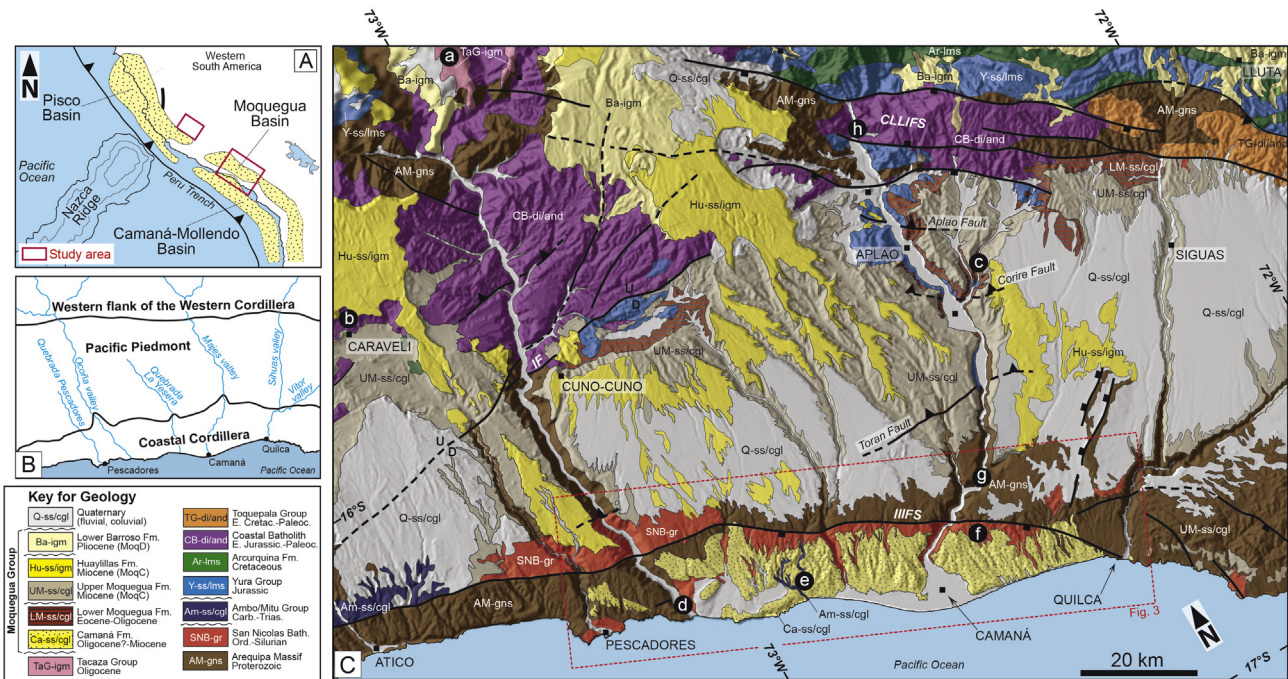


**Fig. 1.** Geology of the coastal region of Arequipa, southern Peru. A: Spatial relations among Pisco, Camaná, and Moquegua Basins. Red box shows the study area. B: Map showing the three main geomorphologic domains within the area and main valleys across. C: Simplified regional geology of the southwest area of Arequipa (after Vicente, 1989; Schildgen et al., 2009; Acosta et al., 2010a, 2010b, 2010c). Main faults are shown in continuous black lines and inferred in dashed black lines. The Cenozoic Moquegua and Camaná Basins are separated by the Coastal Cordillera. Abbreviations: IF = Iquique fault, IIIFS = Ica-Ilo-Islay Faults System, CLLIFS = Cincha-LLuta-Incapuquio Faults System. White letters a–h on black circles indicate sampling sites of potential source rocks. (For interpretation of the references to colour in this figure legend, the reader is referred to the web version of this article.)

are sensitive recorders of provenance change (e.g. Mange and Maurer, 1992; Morton and Hallsworth, 1999). In tectonically active settings, changes in heavy mineral composition are typically associated with tectonic processes, as demonstrated in various case studies (e.g. Pinto et al., 2007; von Eynatten et al., 2008; Decou et al., 2011; Moreno et al., 2011). The analysis of heavy minerals is considerably enhanced by individual single-grain analytical methods to extract precise petrogenetic and chronological information (von Eynatten and Dunkl, 2012). In this study we are heading to combine new information on sedimentary provenance and chronostratigraphy of the Camaná Formation with a previously published sedimentological-stratigraphical model (Alván and von Eynatten, 2014).

To constrain the timing of uplift of the hinterland of Camaná Basin (i.e. Coastal Cordillera and Western Cordillera), it is needed to precisely the sedimentation ages of the Camaná Formation. U–Pb dating of detrital zircons by laser ablation ICP-MS has become an important tool in provenance analysis and stratigraphic dating (e.g. Jackson et al., 1992; Kosler et al., 2002; Kosler and Sylvester, 2007), and here it is applied for the both purposes. In case of coarse-grained deposits with poor fossil content, precise U–Pb ages of volcanic zircons from ashes or reworked ashes are the best candidates to identify depositional ages or maximum depositional ages of a given siliciclastic deposit when using the youngest age component of the age spectrum (e.g. Bowring and Schmitz, 2003; von Eynatten and Dunkl, 2012). U–Pb zircon ages usually express magmatic crystallization and are less sensitive to post emplacement lower temperature metamorphic processes (Cherniak and Watson, 2000). Accordingly, we expect to obtain the crystallization age of plutonic and metamorphic rocks in southern Peru. The older age components of the detrital zircon age spectra provide additional constraints on the provenance of the Camaná Formation.

For the first time, mineral chemistry of titanite is used for provenance discrimination because of its relative abundance and variable colors and composition observed in Camaná Formation. Titanite is a common accessory mineral in igneous (i.e. syenites, diorites, and granites) and metamorphic rocks that are rich in calcium and ferromagnesian minerals (Deer et al., 1982; Franz and Spear, 1985; Frost et al., 2000). Titanite is like zircon suitable for U–Pb geochronology because of its relative high Th and U contents, and its high closure temperature for Pb diffusion (650 °C–700 °C, Cherniak, 1993; Scott and St. Onge, 1995; Frost et al., 2000; Sun et al., 2012). It tends to concentrate wide spectra of trace elements which are well-suited for discrimination of titanite from different source rocks (e.g. (Frost et al., 2001; Aleinikoff et al., 2002; Sun et al., 2012)). Titanite is expected to keep its original crystal chemical composition from the source rock due to its relative resistance to chemical weathering (Morton, 1991; Mange and Maurer, 1992).

## 2. Geologic setting of the southern Peruvian forearc

Since ca. Late Jurassic, convergence and variations in obliquity and subduction rate of the Nazca plate beneath the South American continent have triggered shortening of the Central Andes (Pitcher et al., 1985; Isacks, 1988; Sobolev and Babeyko, 2005; Oncen et al., 2006; Wipf, 2006). During Cenozoic two major phases of deformation during Cenozoic have been described (Isacks, 1988; Allmendinger et al., 1997; Kay et al., 1999; Oncen et al., 2006). At ~40 or ~35 Ma strong decrease of convergence rate, fragmentation of the slab, and initiation of flat subduction caused strong interplate coupling, crustal shortening, uplift, and decrease in volcanic activity (Somoza, 1998; Gilder et al., 2003; Oncen et al., 2006; Mamani et al., 2010; Martinod et al., 2010; Decou et al., 2013).

This phase lasted until ~25 Ma, when the slab became steep again and voluminous magmatism has restarted (Huayllillas volcanic arc, Mamani et al., 2010; see Section 2.1). Many studies have recognized the onset of a second major episode of uplift in southern Peru and Bolivia at ~10 Ma (Schildgen et al., 2007; Thouret et al., 2007; Garzione et al., 2008). This episode is related to several important changes in e.g. convergence style, crustal processes and volcanism, and is thought to have triggered major onset of valley incision (see Section 5.5).

Further evidence of shortening and uplift is documented in numerous fault systems in southern Peru (e.g. Jordan et al., 1983; Jacay et al., 2002; Carlotto et al., 2009). These faults systems include the Cincha-LLuta-Incapuquio Faults System (CLLIFS) and the Ica-Islay-Ilo Faults System (IIIFS) (Vargas, 1970; Vicente, 1989; Jacay et al., 2002; Carlotto et al., 2009; Acosta et al., 2010a) (Fig. 1C). These faults follow the general ~NW–SE-striking alignment of Proterozoic, Paleozoic, and Mesozoic rocks (Palacios and Chacón, 1989; Palacios et al., 1993) forming the main geomorphologic domains of western southern Peru i.e. Western Cordillera and Coastal Cordillera (Pecho and Morales, 1969; Jacay et al., 2002) (Fig. 1B).

## 2.1. Basement and Paleozoic to Mesozoic strata of Western and Coastal Cordilleras

Along the Western Cordillera and the Coastal Cordillera, metamorphic, igneous, and sedimentary rocks are exposed (Cobbing et al., 1977; Bellido and Narváez, 1960; Pecho and Morales, 1969). Metamorphic rocks consist of migmatites, amphibolites, and epidote-bearing gneisses known as the Arequipa Massif (García, 1968; Pecho and Morales, 1969; Cobbing and Pitcher, 1972; Shackleton et al., 1979; Loewy et al., 2004; Chew et al., 2008). The Arequipa Massif is Proterozoic in age (Cobbing et al., 1977) and both the Western Cordillera and the Coastal Cordillera comprises rocks of this lithological unit (Fig. 1C). Abundant garnet-rich granulites, sillimanite-bearing gneisses, and high-Al migmatites (Shackleton et al., 1979; Martignole and Martelat, 2003) characterize the Arequipa Massif in the Coastal Cordillera. Igneous rocks of the Ordovician-Silurian San Nicolas Batholith crops out solely in the Coastal Cordillera along the IIIFS (Cobbing et al., 1977; Acosta et al., 2010b, 2010c).

In Coastal Cordillera, remnants of Carboniferous marine siltstones of the Carboniferous Ambo Group (Acosta et al., 2010b) and Triassic quartzarenites and conglomerates of the Mitu Group (Pecho and Morales, 1969) crop out NW of Camaná (Fig. 1C). Sandstones and limestones of the Jurassic Yura Group crops out from the western flank of the Western Cordillera to the Altiplano (Jenks and Harris, 1953; Benavides, 1962; Vargas, 1970).

## 2.2. Magmatism

Magmatism in southern Peru and northern Chile occurred in different stages. During Ordovician to Silurian, the San Nicolas Batholith has intruded the Arequipa Massif between Camaná and Atico, emplacing calc-alkaline red granites and syenogranites (Bellido, 1969; Cobbing and Pitcher, 1972; Cobbing et al., 1977; Mukasa and Henry, 1990; Loewy et al., 2004; Mamani et al., 2012). Between Early Jurassic and Paleocene, episodic magmatism occurred along the Western Cordillera (Tosdal et al., 1981; Mukasa, 1986; Boily et al., 1989). Cobbing et al. (1977) grouped these occurrences and summarized them as Coastal Batholith. They consist of distinct suites of calc-alkaline and subalkaline “I” type plutons and volcanic rocks (Mamani et al., 2010). The latest emplacement occurred at ~75 to ~55 Ma (Toquepala Group, Cobbing and Pitcher, 1979; Mukasa, 1986; Mamani et al., 2012). It consists of a wide

range of voluminous subalkaline intrusions characterized by K-rich igneous rocks such as diorites, granodiorites, basalts to andesites, and rhyolites (Martínez and Cervantes, 2003; Mamani et al., 2010).

According to Mamani et al. (2010) magmatism restarted around ~30–3 Ma when the slab became steeper again. These author suggested that Cenozoic magmatism is grouped by chemistry and chronology into the ~30–24 Ma Tacaza arc (or Tacaza Group by Wilson and García, 1962), the ~24–10 Ma Huayllillas arc (or Huayllillas Formation by Wilson and García, 1962), and the ~10–3 Ma Lower Barroso volcanic arcs. Cenozoic volcanism was active during sedimentation in the forearc (Marocco and Noblet, 1990; Decou et al., 2011). At present day, the magmatic arc is located in the Western Cordillera and the Altiplano of southern Peru and northern Chile (Mamani et al., 2010).

## 2.3. Cenozoic sedimentary basins

The Moquegua Basin is located along the internal forearc of southern Peru (or Pacific Piedmont, between the Western Cordillera and the Coastal Cordillera, Fig. 1B) and extends further south into northern Chile (Azapa Formation, Salas et al., 1966; Wotzlaw et al., 2011). The Moquegua Group consists of alluvial, fluvial, and lacustrine deposits ranging from Eocene (~50 Ma) to Pliocene (~4 Ma) in age (Marocco et al., 1985; Sempere et al., 2004; Decou et al., 2011). They reflect provenance from the Western Cordillera and the Altiplano (Decou et al., 2013). We follow the sub-division of Sempere et al. (2004) with refinements of Decou et al. (2011), where the Moquegua Group consists of four units i.e. MoqA (~50–40 Ma), MoqB (~40–30 Ma), MoqC (~30–15/10 Ma), and MoqD (~15/10–4 Ma). The MoqC and MoqD units are the only units that show evidence of intense volcanism derived from southern Peru and/or northern Chile (Mamani et al., 2010; Decou et al., 2011).

At the western flank of the Coastal Cordillera, the Camaná Basin (Fig. 1B) contains the Camaná Formation (Rivera, 1950; Rüegg, 1952; Pecho and Morales, 1969; PERUPETRO, 2003). It forms a ~NW–SE striking sedimentary deposit elongated along the coast between Pescadores (16°25'S) and Punta del Bombón (17°15'S) (Fig. 1C), and extends offshore to the outermost forearc (Macharé et al., 1986; PERUPETRO, 2003). According to Alván and von Eynatten (2014), the Camaná Formation is divided into two depositional units, CamA and CamB based on facies analysis. CamA unit consists of coarse-grained deltaic deposits and CamB consists of fluvial conglomerates. CamA is further sub-divided into sub-units A1, A2, and A3 (Alván and von Eynatten, 2014) (Fig. 2). Sub-unit A1 consists of mouth bars and distributary channels. Sub-unit A2 consists of progradational clinothems. Sub-unit A3 consists of delta front to prodelta deposits arranged in onlapping deposits and locally interbedded with fluvial conglomerates in proximal sites. The CamB unit consists of fluvial conglomerates with thin marine intercalations at its base. Previous literature and facies analysis permitted to present a preliminary chrono-stratigraphic framework (Alván and von Eynatten, 2014, and references therein) and suggest that the Camaná Formation is Late Oligocene to Late Miocene in age.

According to Alván and von Eynatten (2014), the sub-units A1 and A2 represent a regressive systems tract, and strongly contrasts to the Early to Middle Miocene global transgression of Haq et al. (1987). This suggests significant uplift of the Coastal Cordillera during deposition of A1 and A2. Deposition of sub-unit A3 occurred during a transgressive systems tract and it is consistent with the end of that global sea-level rise. This statement suggests that only minor tectonic influence occurred at this stage. Sedimentation of CamB occurred during a later regression (Late Miocene). Nonetheless, the study area is widely influenced by strong pulses of uplift in Late Miocene (i.e. in Western Cordillera and Altiplano) (cf.

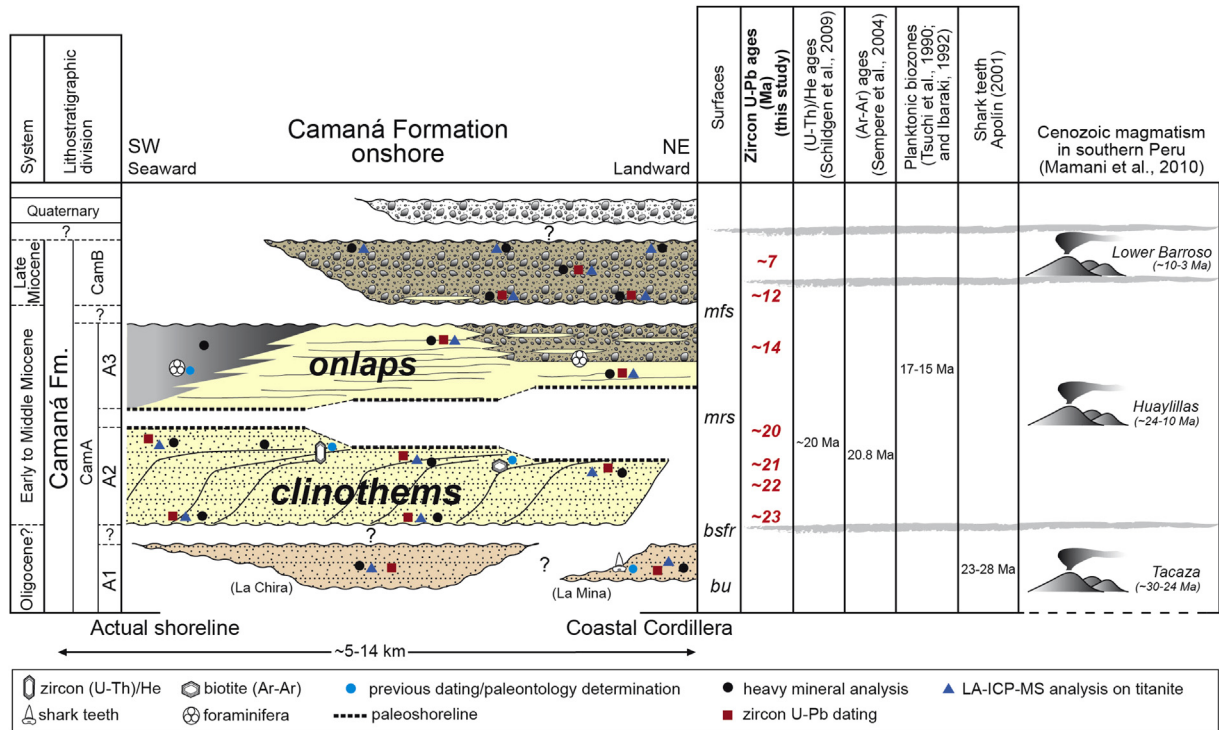


**Fig. 2.** Wheeler-type diagram for the Camaná Formation. The Camaná Formation is divided into CamA unit (sub-units A1, A2, and A3) and CamB unit (Alván and von Eynatten, 2014). New ages (red numbers) are obtained by U–Pb geochronology of zircon from reworked ash (see Table 1 and Fig. 4). Blue dots indicate position of previous dating. Black dots indicate sampling for heavy mineral analysis. Blue triangles indicate sampling for LA-ICP-MS analysis on titanites. Red boxes indicate sampling for U–Pb dating. Abbreviations: bu = basal unconformity, bsfr = basal surface of forced regression, mrs = maximum regressive surface, mfs = maximum flooding surface. (For interpretation of the references to colour in this figure legend, the reader is referred to the web version of this article.)

Onccken et al., 2006; Thouret et al., 2007; Garzzone et al., 2008; Schildgen et al., 2009).

### 3. Sampling and methods

We collected igneous and metamorphic rocks from potential source areas and sedimentary samples from the Camaná Formation. Potential source rocks were collected from eight sites along the Western Cordillera and the Coastal Cordillera (indicated by white letters on black circles in Fig. 1C). Some of these source rocks are represented by pebble population samples following the approach of Dunkl et al. (2009). Samples of the Camaná Formation (CamA unit: A1, A2, A3, and CamB unit) have been collected from nine sites (white numbers on black circles in Fig. 3B). In order to obtain provenance information, we performed (i) U–Pb geochronology of detrital zircons (17 samples) and detrital titanites (9 samples), (ii) heavy mineral analyses of parental (10 samples) and sedimentary rocks (21 samples), and (iii) single grain geochemical analyses on parental (4 samples) and detrital titanites (12 samples) by laser ablation ICP-MS technique. To obtain stratigraphic ages, we considered the youngest age components of the U–Pb geochronology.

Following the method of Hutton (1950) and Mange and Maurer (1992) the samples were crushed with a jaw-crusher and sieved. Two fractions are selected for our analysis, 63–250 µm and 63–125 µm, and the carbonate was dissolved in 5% acetic acid. For geochronology, the density separation was performed on the fraction 63–250 µm using sodium metatungstate ( $\rho = 2.87 \text{ g/cm}^3$ ). The heavy mineral fractions were further separated using the Frantz magnetic separator at 0.5–1.0 A with 10° side tilt in order to enrich the zircon and titanite grains. Thereafter, individual grains of zircon and titanite were hand-picked under the microscope and mounted

in epoxy resin, then grinded and diamond polished in five steps down to 1 µm. For the properly exposed zircon grains, we obtained cathodoluminescence images by using a JEOL JXA 8900 electron microprobe at the Geoscience Center of the Georg-August University, Göttingen. These images permitted studying the internal structure of the crystals and select homogeneous parts for the in-situ geochronology. The zircon U–Pb measurements were carried at the Institute of Geosciences, Frankfurt (Germany) using an excimer laser ablation system (Resonetics) coupled to an Element2 sector field ICP-MS (Kosler and Sylvester, 2007; Gehrels et al., 2008; Frei and Gerdes, 2009). Individual zircons were selected randomly from all sizes and shapes, but avoiding zircons with huge inclusions. In some samples the numbers of usable grains were rather limited (see Section 4.1). Previous studies on sedimentary provenance have shown that a high number of single grains (>100) is necessary to ensure that even small (~5%) components (e.g., a detrital age spectrum) are not missed at 95% confidence level (Vermeesch, 2004). However, such a large amount of zircons is difficult to obtain even from large samples (>3 kg) of the Camaná Formation.

The age calculation is based on the drift- and fractionation correction by standard-sample bracketing using GJ-1 zircon reference material (Jackson et al., 2004). For further control, we analyzed the Plesovice zircon (Sláma et al., 2008) and the 91,500 zircon (Wiedenbeck et al., 1995) as “secondary standards”. The age results of the standards were consistently within  $1\sigma$  of the published ID-TIMS values. In order to identify the major age components in the complex detrital age spectra we applied different procedures. The TuffZirc procedure (Ludwig, 2003) can find the youngest coherent group of at least 5 age data from at least 12 analyses. In this way both the inherited cores and the Pb loss influenced spot ages can be avoided. The “PopShare” (Dunkl and

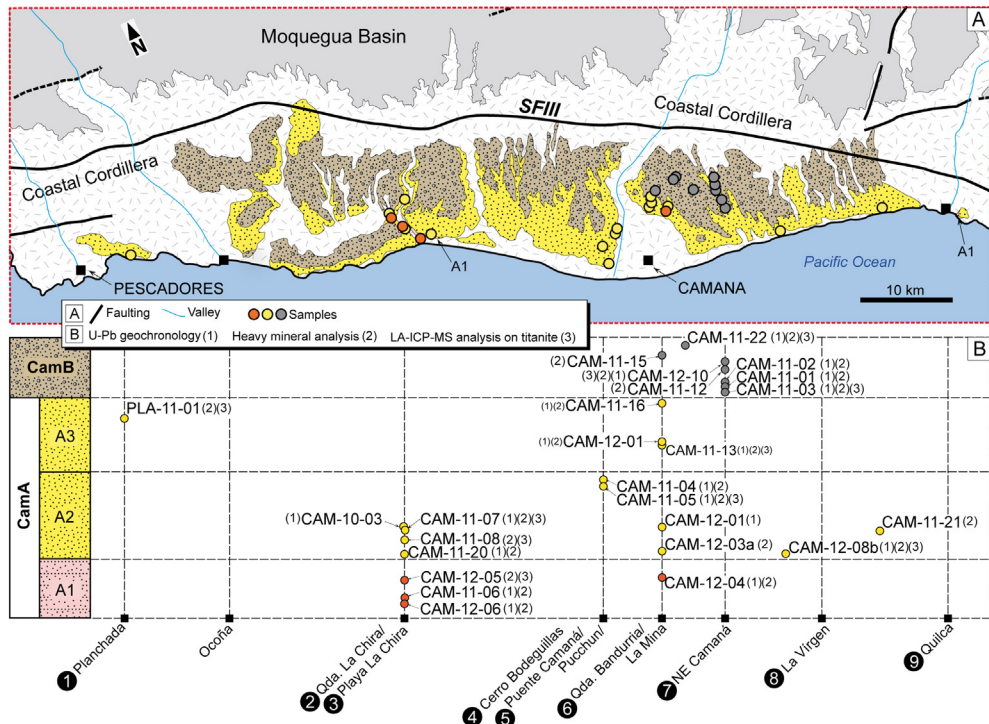


**Fig. 3.** Detailed scheme of the local geology between 16°25'S and 17°15'S. A: Geological map and location of the samples for this study. B: Simplified stratigraphy of the Camaná Formation (Alván and von Eynatten, 2014) and a rough stratigraphic position of the samples. The study sites are indicated in white numbers on black circles.

Székely, 2002) and the “Density plotter” software (Vermeesch, 2012) are based on different algorithms and can identify more age components. We assigned the highest relevance to the youngest age components as they provide the most reliable maximum age of deposition (von Eynatten and Dunkl, 2012). The different procedures yield very similar ages for the youngest age components, with discrepancies usually in the range of only a few 100 ky. We performed U-Pb dating of zircons from 17 samples, dating usually 50 to 60 grains per sample (implying that age components of 10% or more should be covered at 95% confidence level). In some samples (e.g. samples CAM-11-08 and CAM-11-06), we dated only 15 to 30 grains because the zircon concentration in these samples did not allow more measurements. In some cases, samples derived from the same stratigraphic level were merged to achieve better stratigraphic significance and more robust identification of age clusters (i.e. samples CAM-11-02, CAM-11-03, CAM-11-01, CAM-12-10 and samples CAM-11-07, CAM-10-03, Table 1) (see Section 4.1).

Due to its high closure temperature (550–650 °C), the titanite U–Pb ages can be interpreted as igneous crystallization ages or cooling ages following the emplacement of deep intrusions or cooling under upper amphibolite facies conditions (Aleinikoff et al., 1993; Frost et al., 2000). We dated colorless and pale green titanites by U–Pb geochronology considering between 2 and 10 grains per sample because most of grains were relatively small and not suited for dating. Like in case of zircons, the titanite ages from some samples were merged if they derive from the same stratigraphic level (i.e. samples CAM-11-01, CAM-12-10, CAM-11-03, CAM-12-01).

In order to achieve unbiased heavy mineral spectra, we performed gravity separation on the fraction 63–125 µm after acetic acid treatment. Around ~20 mg was extracted from each sample, and placed on a paper slide using a small funnel (to avoid fractionation). Samples were split in four equal parts using a razor blade, where a quarter of the sample (~5 mg) is mounted on a glass

slide and embedded with “Cargille Meltmount” (refraction index of 1.66) at ca. 70 °C. Quantitative ribbon-counting of heavy minerals was performed counting 250 to 300 non-opaque grains per slides. We analyzed the heavy mineral composition of sedimentary samples from the Camaná Formation to compare them with the potential source rocks spectra. Additionally, the optical analysis of some samples was reinforced by Raman spectroscopy. The Raman spectra were evaluated by the software CrystalSleuth (Laetsch and Downs, 2006). The in-situ geochemical analysis of titanite grains was completed at the Geoscience Center of the Georg-August University, Göttingen, using an excimer laser coupled to a Perkin Elmer DRC II ICP-MS.

## 4. Results

### 4.1. Detrital zircon and titanite U–Pb geochronology

In total, this section presents 595 new zircon U–Pb ages and 97 titanite U–Pb ages. The results are listed in Table 1, and they are graphically presented as binned frequency plots and probability density plots constructed by AgeDisplay (Sircombe, 2004) (Figs. 4 and 5).

In sub-unit A1 of CamA unit the zircon single-grain age spectra ( $n = 70$  ages) are dominated by Silurian U–Pb age components (~440–~430 Ma) and no Cenozoic ages were detected (see Fig. 5A). However, in sub-unit A2 ( $n = 201$  ages) and sub-unit A3 ( $n = 106$  ages) beyond the early Paleozoic zircon ages, Cenozoic ages are present. The youngest age components are  $23.0 \pm 0.4$  Ma (Playa La Chira, Figs. 4A), and  $21.7 \pm 1.3$  Ma (Quebrada La Chira, Fig. 4B) at the base of the sub-unit A2, and  $21.2 \pm 0.5$  Ma (Playa La Virgen, Figs. 4C) and  $20.0 \pm 0.6$  Ma (Puente Camaná, Fig. 4D) near the topmost strata of sub-unit A2. These age components can be considered as maximum age of sedimentation. Furthermore, zircons from the topmost strata of A3 yield a youngest age component of

**Table 1**

Zircon and titanite U–Pb data including sample description and location. Youngest zircon age components and single-grain ages on zircons and titanites >24 Ma. N.C. (Zrn) = number of zircon crystals, N.C. (Ttn) = number of titanite crystals. Total number of zircons dated is 595, and total number of titanites dated is 97. Plus (+) symbol in samples at CamB unit indicates merging of samples.

Sample	Stratigraphy	Description	UTM E	UTM N	alt. (m)	Youngest age component	"Old" single-grain ages and age component			
							N.C. (Zrn)	Age ± 2σ (Ma)	N.C. (Zrn)	Age ± 2σ (Ma)
CAM-11-22	upper CamB	Quebrada Bandurria	751239	8165802	604	39	7.5 ± 0.4	4	-86–240	
							2	-435–470		
							5	-960–1650		
CAM-12-10+	lower CamB	Panamerican highway, SE Camaná	752944	8165123	492	136	12.4 ± 0.3	2	-65–70	1 ~10
CAM-11-02+			753071	8164820	460			7	-120–280	7 ~34–85
CAM-11-01+			753066	8164772	457			3	-460–480	10 ~290–480
CAM-11-03			752746	8162688	311			20	-950–1870	
CAM-11-16	upper A3	Quebrada Bandurria	746510	8165376	390	15	13.6 ± 0.4	1	-400	
							5	-1200–1730		
CAM-12-01	lower A3	La Mina	746661	8166096	417			29	451.6 ± 3.8	1 ~52
								8	432.0 ± 3.9	
CAM-11-13	lower A3	Quebrada Bandurria	746715	8166116	449			56	460.8 ± 6.1	19 392.7 ± 10.0
CAM-11-05	upper A2	Puente Camaná	741936	8165130	46	6	20.0 ± 0.6	46	434.2 ± 6.7	18 408.7 ± 13.6
CAM-12-08b	A2	Playa La Virgen	756628	8155804	26	10	21.2 ± 0.5	3	-450	
							8	-990–1790		
CAM-11-07+	lower A2	Quebrada La Chira	720591	8175087	156	10	21.7 ± 1.3	56	458.3 ± 4.5	10 420.1 ± 9.1
CAM-10-03							4	-1140–1820		
CAM-11-08	lower A2	Quebrada La Chira	720460	8175211	179	5	~18 to ~33	1	1801	
CAM-11-20	lower A2	Playa La Chira	722011	8172689	19	6	23.0 ± 0.4	1	-136	
							42	457.4 ± 5.6		
							3	-1140–2170		
CAM-12-04	A1	La Mina	745810	8163672	79			27	437.6 ± 4.9	11 433.3 ± 6.5
CAM-11-06	A1	Quebrada La Chira	720580	8175114	167			17	433.5 ± 5.9	
							1	-1710		
CAM-12-06	A1	Playa La Chira	721880	8172638	3			25	439.0 ± 6.5	12 424.8 ± 11.2
Total						227		368		97

13.6 ± 0.4 Ma (Quebrada Bandurria, Fig. 4E). Zircon U–Pb age components and single-grain ages >24 Ma are also abundant in these sub-units, showing signals between ~460 and ~434 Ma and subordinate ages between ~2170 and ~990 Ma (Table 1 and Fig. 5B to E).

The amount of zircons from reworked ash layers in the sandy sediments of CamB ( $n = 218$  ages) is higher than in sediments of CamA (specifically the sub-units A2 and A3). Zircons at the base of the CamB unit ( $n = 169$  ages) yield the youngest U–Pb age components of  $12.4 \pm 0.3$  Ma (NE Camaná, Figs. 4F), and  $7.5 \pm 0.4$  Ma near the top of CamB unit (Quebrada Bandurria, Fig. 4G). The youngest age component shown in Fig. 4F ( $12.4 \pm 0.3$  Ma) is a result of 136 combined data by using the TuffZirc algorithm (ISOPLOT software, Ludwig, 2003). However, using other algorithms like Density Plotter (Vermeesch, 2012) and PopShare (Dunkl and Székely, 2003) we obtained even younger age components like 8.7, 9.1, and 9.8 Ma using different settings for the search algorithms (see Section 5.1). It poses the possibility that the maximum age of deposition of CamB is younger than 10 Ma.

In the spectrum of CamB unit, zircon U–Pb ages of single grains older than 24 Ma are also observed, and they consist of abundant ages between ~1870 and ~950 Ma, and in minor proportion single-grain ages between ~480 and ~435 Ma, between ~280 and ~85 Ma, and between ~30 and ~24 Ma (Table 1 and Fig. 5F). Additionally, we observe few titanite U–Pb single-grain ages between ~480 and ~290 Ma, and between ~85 and ~34 Ma (blue lines in Fig. 4F). For discussions and interpretations, we have separated our geochronological results in two sections: (i) the youngest zircon age components <24 Ma relevant for the chronostratigraphy of Camaná Formation (see Section 5.1), and (ii) the ages older than 24 Ma, comprising zircon and titanite ages with high relevance for the provenance model (see Section 5.3).

## 4.2. Heavy mineral analysis

The heavy mineral spectra are presented in Table 2 and Figs. 6 and 7. Abbreviations of heavy minerals have been taken from Whitney and Evans (2010), Zrn = zircon, Tur = tourmaline, Rt = rutile, Ap = apatite, Pxn = pyroxene, Sil = sillimanite, and Ep = epidote. Besides the usual abbreviations we introduced for the special varieties Ttn<sub>1</sub> = brown/yellow titanite, Ttn<sub>2</sub> = colorless/pale green titanite, Grt<sub>1</sub> = pink garnet, Grt<sub>2</sub> = colorless/pale green garnet, Amp<sub>1</sub> = fresh amphibole, and Amp<sub>2</sub> = altered amphibole. Commonly used heavy mineral ratios were also considered in our analysis in order to characterize mineral spectra (e.g. ZTR = zircon-tourmaline-rutile index, GZi = garnet-zircon index, and ATI = apatite-tourmaline index, according to Hubert, 1962; Morton and Hallsworth, 1999).

### 4.2.1. Heavy mineral spectra of potential source rocks

Optical examination of heavy minerals from potential source lithologies (Fig. 6) allows characterizing their composition, and provides the basis for comparisons with the Camaná Formation. Potential source rocks are restricted to the rocks forming the Coastal Cordillera and the Western Cordillera (white letters on black circles in Fig. 1C). Potential source rocks are the Arequipa Massif (gneisses, granulites, and migmatites), the San Nicolas Batholith (granites), the Coastal Batholith (diorites), the Mitu Group (conglomerates and quartzarenites), the Yura Group (quartzarenites), and the Tacaza Group (diorites) (Table 2A).

**4.2.1.1. Arequipa Massif.** The metamorphic rocks of the Arequipa Massif crop out in the Coastal Cordillera and the Western Cordillera. These rocks consist of Greenvillian-aged metamorphic rocks collected in north of Aplao and in Toran (sites "h" and "g" in Fig. 1C). The representative heavy mineral spectrum of the Arequipa Massif

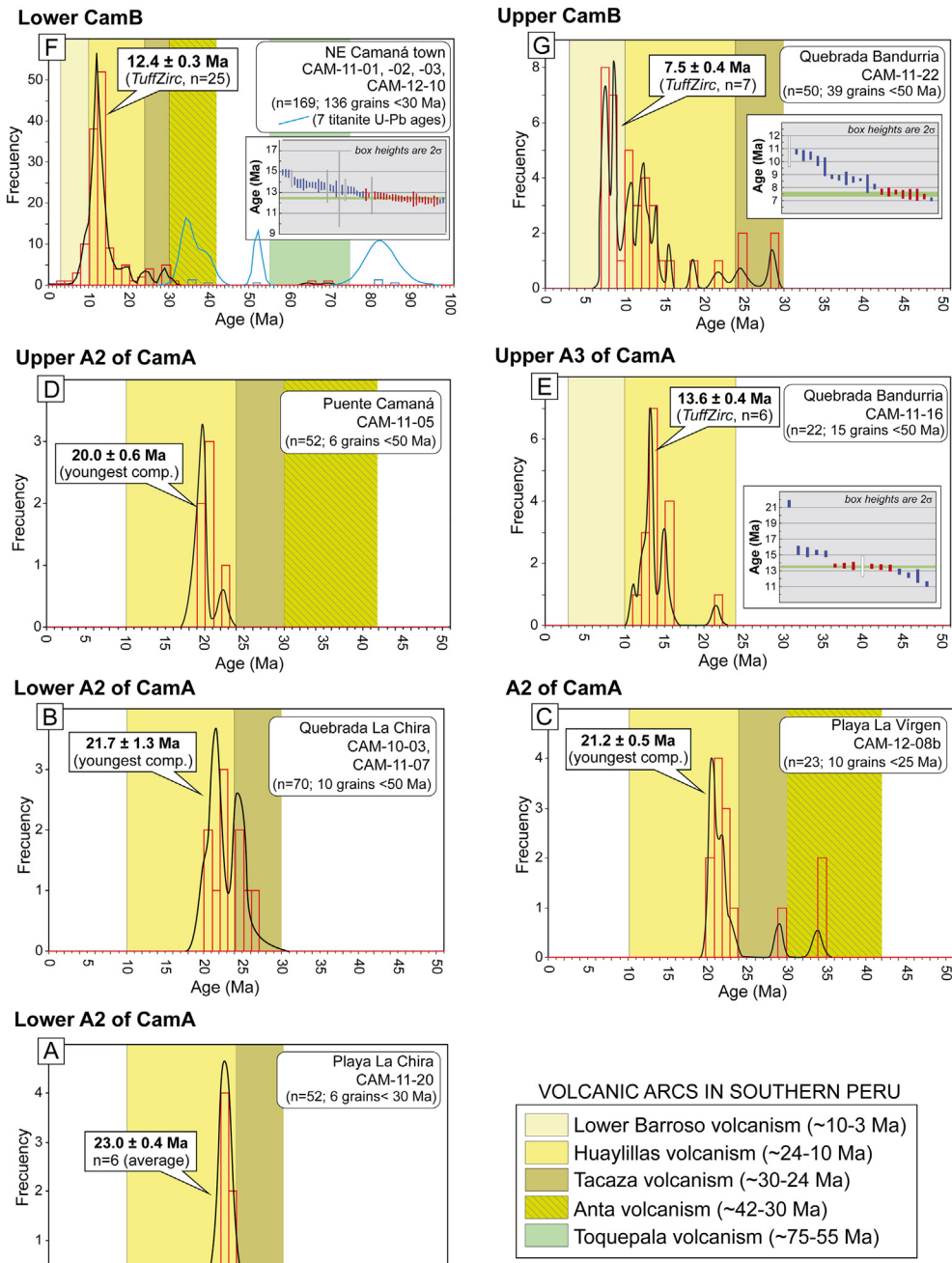


**Fig. 4.** Binned age histograms and probability density plots of zircon (red and black lines) and colorless titanite (blue) single-grain U–Pb ages obtained on the Camaná Formation. The probability density plots were calculated by *AgeDisplay* and *Density Plotter* softwares (Sircombe, 2004; Vermeesch, 2012). The youngest age components were identified by *Density Plotter* or by *PopShare* methods (Vermeesch, 2012; Dunkl and Székely, 2002). When the number and quality of single-grain ages allowed then the youngest component was identified by the *TuffZirc* method (Ludwig, 2003). Red vertical bars on the cumulative plots indicate the single-grain ages that are considered for the *TuffZirc* age. (For interpretation of the references to colour in this figure legend, the reader is referred to the web version of this article.)

shows  $\text{Grt}_1$  (up to 69%), and  $\text{Ep}$  (up to 70%) and they are considered as major components.  $\text{Ap}$  (up to 17%),  $\text{Sil}$  (6%), and  $\text{Ttn}_2$  (up to 7%) are also observed as subordinate components. Notably,  $\text{Grt}_1$  and  $\text{Sil}$  are only found in the granulites and migmatites of the Arequipa Massif of the Coastal Cordillera (site “g” in Fig. 1C), as observed by Martignole and Martelat (2003); while gneisses of the Arequipa Massif within the Western Cordillera contain  $\text{Grt}_2$  (site “h” in Fig. 1C) and are rich in  $\text{Ep}$  and  $\text{Amp}_2$ . The proportions of  $\text{Pxn}$ ,  $\text{Zrn}$ ,

$\text{Tur}$ , and  $\text{Rt}$  are very minor (their sum is 12%), while  $\text{Amp}_1$  and  $\text{Ttn}_1$  are not observed.

**4.2.1.2. San Nicolas Batholith.** The igneous rocks of the San Nicolas Batholith crop out at the Coastal Cordillera and they consist of red granites and syenogranites. The samples were collected northeast of the town of Camaná (site “f” in Fig. 1C). The heavy mineral assemblage shows  $\text{Ttn}_1$  (78%) and  $\text>Zrn}$  (11%) as major components.

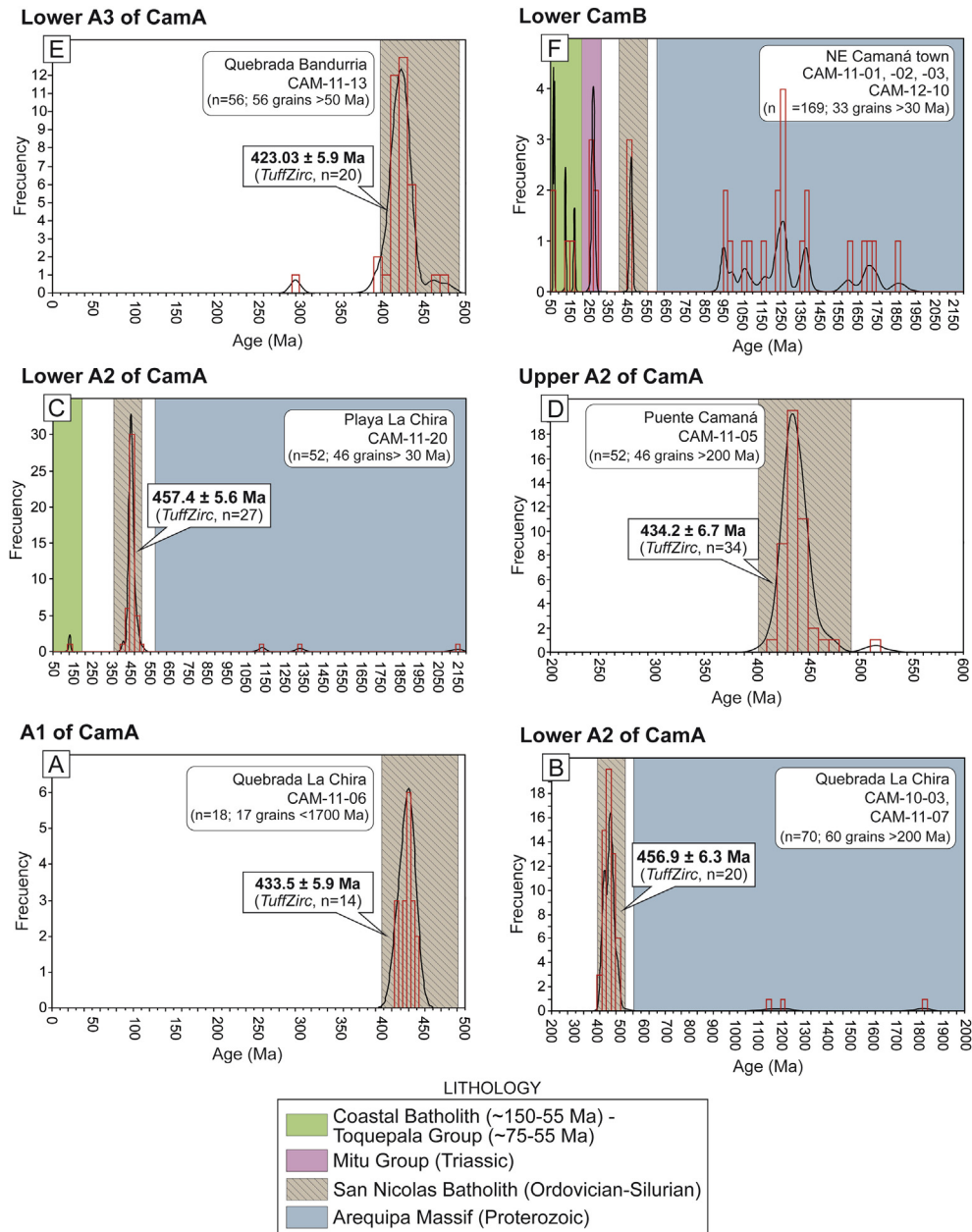


**Fig. 5.** Zircon U–Pb age components and single-grain ages of potential source rocks. Ages are shown in binned age histograms and probability density plots (red and black lines). We used *AgeDisplay* and *Density Plotter* softwares (Sircombe, 2004; Vermeesch, 2012) for age calculations. (For interpretation of the references to colour in this figure legend, the reader is referred to the web version of this article.)

Ttn<sub>1</sub> is only observed in granites and syenogranites of the San Nicolas Batholith (see Section 4.3.1 and Fig. 8). Minor components include Ap (5%), Amp<sub>2</sub> (3%), and Gr<sub>1</sub> (<1%). Sil, Amp<sub>1</sub>, Grt<sub>2</sub>, Rt, Pxn, Tur, and Ttn<sub>2</sub> are not observed.

**4.2.1.3. Coastal Batholith.** The igneous rocks of the Coastal Batholith crop out at the northeast side of the study area (Western Cordillera). They are diorites collected near Caravelí (sites "b" and "c" in Fig. 1C). The representative heavy mineral concentration shows Amp<sub>1</sub> (up to 84%) and Ep (up to 15%) as major components. Subordinate components are Amp<sub>2</sub> (5%). The proportions of Ap, Zrn, Pxn, and Ttn<sub>2</sub> are very minor or not significant (the sum is 5%). Sil, Tur, Rt, Grt<sub>1</sub>, Grt<sub>2</sub>, and Ttn<sub>1</sub> are not observed.

**4.2.1.4. Mitu, Yura, and Tacaza Groups.** Quartzarenites of the Mitu and Yura Groups crop out mostly along the Western Cordillera. We collected pebbles of quartzarenites at the river mouth of the Ocoña valley (site "d" in Fig. 1C). The quartzarenites show abundance of Zrn (75%) and Rt (20%), and subordinate proportions of Ap, Pxn, Grt<sub>1</sub>, Ep, Amp<sub>2</sub>, and Tur (between 1% and 4%). The concentration of ZTR minerals (Zrn, Tur, and Rt) suggests a high-degree of mineralogical maturity. Diorites of the Tacaza Group crop out in the Altiplano and the Western Cordillera, and we collected samples at Cotahuasi, northeast Caravelí (site "a" in Fig. 1C). Diorites show Ep (47%), Amp<sub>2</sub> (26%), and Pxn (21%) and they are considered as major components of the Tacaza Group. The high proportion of Pxn is conspicuous of the Tacaza Group, and also the Huayllillas and Lower Barroso volcanic arcs (Decou et al., 2011). Proportions of Ttn<sub>2</sub> (up to

**Table 2**

Heavy mineral compositions of the potential source rocks (A) and the Camaná Formation (B). Values are expressed in percentages. To see location of sampling of potential source rocks, see Fig. 1, and location of samples of the Camaná Formation, see Fig. 3. All samples listed in both tables have been analyzed for heavy minerals, and additional analysis are indicated in columns at the right side, where 1 = U–Pb on zircons, 2 = U–Pb on titanites, and 3 = LA-ICP-MS analysis of titanites. Sample CAM-11-01 (not listed here) has been processed for zircon and titanite U–Pb geochronology and joined to the samples CAM-11-02, CAM-11-03, and CAM-12-10 (Fig. 4F). Sample CAM-10-03 (not listed here) has been processed for zircon U–Pb geochronology and joined to the sample CAM-11-07 (Fig. 4B) (see Section 4.1). Abbreviations: Zrn = zircon, Tur = tourmaline, Rt = rutile, Ap = apatite, Pxn = pyroxene, Ttn<sub>1</sub> = brown/yellow titanite, Ttn<sub>2</sub> = colorless/pale green titanite, Grt<sub>1</sub> = pink garnet, Grt<sub>2</sub> = colorless/pale green garnet, Sil = sillimanite, Ep = epidote, Amp<sub>1</sub> = fresh amphibole, and Amp<sub>2</sub> = altered amphibole.

A: Potential source rocks																							
Lithology	Sample	Site	Zrn	Tur	Rt	Ap	Pxn	Ttn <sub>1</sub>	Ttn <sub>2</sub>	Grt <sub>1</sub>	Grt <sub>2</sub>	Sil	Ep	Amp <sub>1</sub>	Amp <sub>2</sub>	1	2	3					
Tacaza Group (Oligocene)	TAZ-00-03	a	0	0	0	0	21	0	6	0	0	0	47	0	26	x							
Coastal Batholith (Early Jurassic-Paleocene)	CARA-08-03	b	1	0	0	1	0	0	1	0	0	0	14	77	5	x							
Yura Group (Jurassic)	OCO-08-03	d	75	3	12	1	0	0	0	0	0	0	11	84	0								
Mitu Group (Perm.-Trias.)	CAM-11-11	e	65	3	20	4	2	0	0	2	0	0	4	0	1								
San Nicolas Batholith (Ord.-Sil.)	CAM-08-03	f	11	0	0	5	0	80	0	0	0	0	2	0	2	x							
Arequipa Massif (Proterozoic)	MAJ-12-06	g	0	2	0	1	5	0	0	69	0	6	14	0	3								
	MAJ-12-01A	h	4	0	0	17	0	0	1	0	8	0	35	0	34								
	MAJ-12-01B		0	0	0	3	0	0	6	0	0	0	70	0	20								
	MAJ-12-01D		1	0	0	7	0	0	7	0	0	0	25	0	59	x							
B: Camaná Formation (detrital)																							
Unit	Sample	Site	Zrn	Tur	Rt	Ap	Pxn	Ttn <sub>1</sub>	Ttn <sub>2</sub>	Grt <sub>1</sub>	Grt <sub>2</sub>	Sil	Ep	Amp <sub>1</sub>	Amp <sub>2</sub>	ZTR	ATi	GZi	1	2	3		
CamB	CAM-11-22	8	0	0	0	1	59	0	3	3	0	0	13	0	21	0	1	2	x	x			
	CAM-12-10	8	1	1	2	13	0	10	13	0	1	22	0	28	10	4	7	x	x	x			
	CAM-11-02	6	3	0	3	26	0	1	1	0	0	3	17	41	8	6	0	x					
	CAM-11-12	3	0	1	5	11	1	5	4	0	0	36	0	34	3	5	3						
	CAM-11-03	1	0	0	3	8	0	7	1	0	1	6	2	71	1	3	0	x	x	x			
CamA	A3	PLA-11-01	1	6	0	0	11	2	0	2	5	0	1	6	1	65	6	11	3	x	x		
	CAM-11-16	7	3	0	0	2	3	0	2	2	0	1	13	1	71	4	3	1	x	x	x		
	CAM-12-01	11	0	0	7	0	69	0	4	0	0	3	0	4	11	8	3	x	x	x			
	CAM-11-13	22	0	0	0	10	1	47	0	9	0	0	10	0	1	22	10	4	x	x	x		
	A2	CAM-11-04	6	5	0	14	2	0	46	0	8	2	4	10	0	8	19	3	6				
		CAM-11-05	20	0	0	11	0	33	10	6	0	8	5	3	3	20	11	2	x	x	x		
		CAM-11-21	11	3	2	0	4	1	3	1	42	0	3	8	1	32	5	6	24				
		CAM-12-03a	7	7	0	1	8	0	76	2	0	0	0	5	0	0	9	8	0				
		CAM-12-08b	11	0	0	0	2	1	1	1	0	68	12	12	0	1	0	2	35	x	x		
		CAM-11-08	2	7	3	1	5	2	1	4	0	15	7	54	0	1	11	11	1	x	x	x	
		CAM-11-07	14	0	0	17	4	19	4	1	0	4	5	1	30	14	17	1	x	x	x		
	A1	CAM-11-20	3	15	1	0	9	3	31	0	1	0	3	19	3	13	17	10	10	x			
		CAM-12-05	2	11	2	0	19	0	35	12	3	0	0	16	0	2	13	21	2				
		CAM-12-04	7	4	0	1	10	16	49	1	3	0	0	12	0	4	5	10	2	x	x		
		CAM-11-06	2	6	0	9	13	0	50	11	4	0	0	1	0	6	15	13	2	x	x		
		CAM-12-06	3	5	0	0	7	3	32	23	0	0	3	25	0	2	5	7	0	x	x		

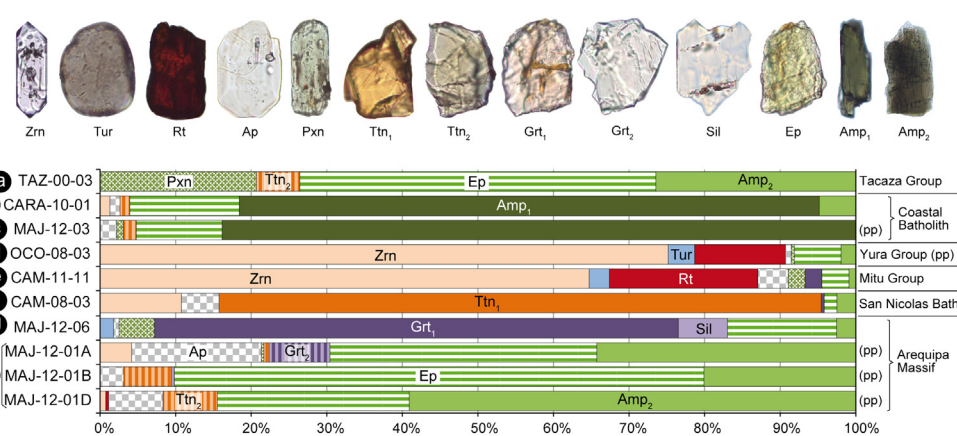


**Fig. 6.** Representative heavy mineral assemblages of potential source rocks. Tacaza Group (Oligocene diorites), Coastal Batholith (Late Cretaceous diorites), Yura Group (Jurassic quartzarenites), Mitu Group (Permian–Triassic quartzites), San Nicolas Batholith (Ordovician–Silurian granites), Arequipa Massif (Proterozoic gneisses and granulites). Grain size varies between 250 and 65 µm. (pp) indicates pebble populations. Lettering in black circles to the left refers to the location of the samples (Fig. 1C). Abbreviations: Zrn = zircon, Tur = tourmaline, Rt = rutile, Ap = apatite, Pxn = pyroxene, Ttn<sub>1</sub> = brown/yellow titanite, Ttn<sub>2</sub> = colorless/pale green titanite, Grt<sub>1</sub> = pink garnet, Grt<sub>2</sub> = colorless/pale green garnet, Sil = sillimanite, Ep = epidote, Amp<sub>1</sub> = fresh amphibole, and Amp<sub>2</sub> = altered amphibole. (For interpretation of the references to colour in this figure legend, the reader is referred to the web version of this article.)

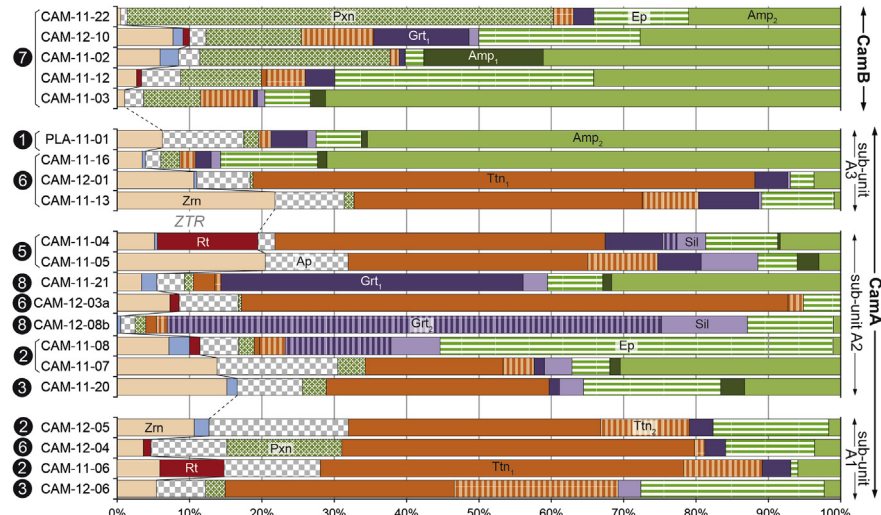


**Fig. 7.** Heavy mineral spectra of the Camaná Formation. Grains counted for each sample are between 200 and 250. The spectra are organized according to four stratigraphic subdivisions, i.e. CamA: A1, A2, A3, and CamB (Alván and von Eynatten, 2014). Location of the samples is indicated in numbers to the left referring to Fig. 3. Abbreviations: Zrn = zircon, Tur = tourmaline, Rt = rutile, Ap = apatite, Pxn = pyroxene, Ttn<sub>1</sub> = brown/yellow titanite, Ttn<sub>2</sub> = colorless/pale green titanite, Grt<sub>1</sub> = pink garnet, Grt<sub>2</sub> = colorless/pale green garnet, Sil = sillimanite, Ep = epidote, Amp<sub>1</sub> = fresh amphibole, and Amp<sub>2</sub> = altered amphibole. (For interpretation of the references to colour in this figure legend, the reader is referred to the web version of this article.)

6%) are considered as subordinate. Ap, Tur, Rt, Ttn<sub>1</sub>, Grt<sub>1</sub>, and Grt<sub>2</sub> are not observed.

#### 4.2.2. Heavy mineral spectra of the Camaná Formation

To describe the heavy mineral spectra of the Camaná Formation (Table 2B), we refer to three main groups, i.e. (i) the sub-unit A1, (ii) the sub-units A2 and A3, and (iii) the CamB unit (Fig. 7), according to the stratigraphic division of Alván and von Eynatten (2014). We consider that the additional use of the ZTR (zircon-tourmaline-rutile), GZi (garnet-zircon), and ATI (apatite-tourmaline) indexes (Hubert, 1962; Morton and Hallsworth, 1999) are appropriate to support the definition of potential provenance shifts.

The heavy mineral spectrum of sub-unit A1 shown in Fig. 7 is dominated by Ttn<sub>1</sub> (up to 50%, sample CAM-11-06), Ep (up to 25%, sample CAM-12-06), Ttn<sub>2</sub> (up to 23%, sample CAM-12-06), Ap (19%, sample CAM-12-05), and Pxn (up to 16%, sample CAM-12-04).

Moreover, subordinate populations include Zrn (up to 11%, sample CAM-12-05), and very minor components of Tur, Sil, Amp<sub>2</sub>, and Grt<sub>1</sub> (less than 6%). Grains of Grt<sub>2</sub> and Amp<sub>1</sub> are not observed in sandstones of the sub-unit A1. The proportion of Rt is commonly minor, except in some layers (up to 9%, sample CAM-11-06). Values of the GZi index in sediments of A1 are the lowest of the Camaná Formation (GZi = 2%); while the ATI values are the highest (between 7% and 21%) (Fig. 9).

Sediments of the sub-unit A2 and lower part of sub-unit A3 show the highest concentration of Ttn<sub>1</sub> observed in the Camaná Formation (up to 76%, sample CAM-12-03a). This amount is followed by Ep (up to 54%, sample CAM-11-08), Zrn (up to 22%, sample CAM-11-13), and Ap (up to 17%, sample CAM-11-07). Despite Grt<sub>1</sub> and Grt<sub>2</sub> are frequently subordinate constituents in these sediments, they are exceptionally abundant in some layers (e.g. Grt<sub>2</sub>, 68%, sample CAM-12-08b; Grt<sub>1</sub>, 42%, sample CAM-11-21; and Ttn<sub>2</sub>,

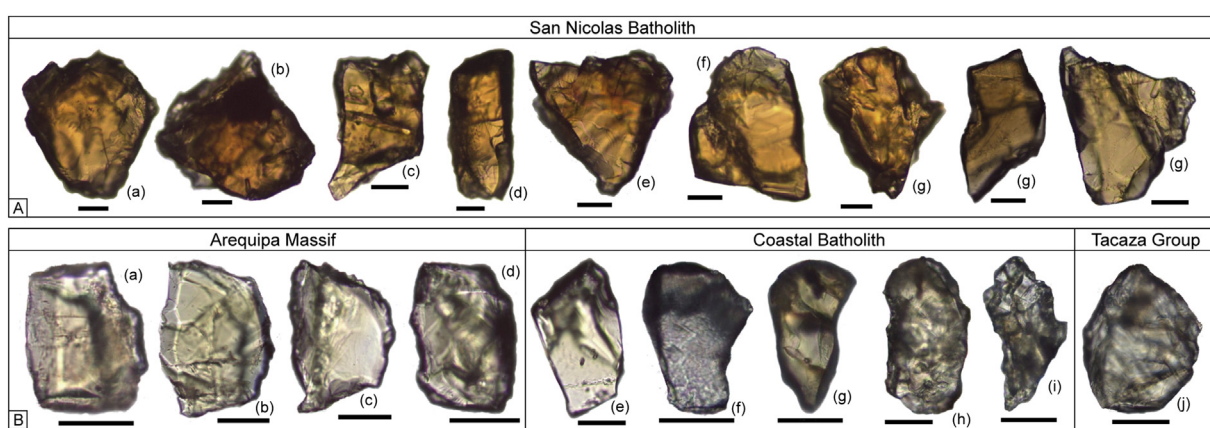


**Fig. 8.** Representative population of titanite grains from source rocks (embedded in Cargile Melmount 1.66). A: Brown/yellow titanite (Ttn<sub>1</sub>) of red granites of the Ordovician San Nicolas Batholith (CAM-08-03), collected ~8 km northeast Camaná town. B: Colorless/pale green titanite (Ttn<sub>2</sub>). (a) to (d) are pebbles derived of the Proterozoic Arequipa Massif and were collected in Majes Valley, ~5 km north of Aplao Town. (e) to (i) Titanite of diorite of the Coastal Batholith collected in Corire (MAJ-12-03), and (i) ~1 km northwest of Caravelí Town (CARA-10-01). (j) Titanite of diorite of the Tacaza Group (TAZ-00-03) collected ~8 km NE Caravelí town. (For interpretation of the references to colour in this figure legend, the reader is referred to the web version of this article.)

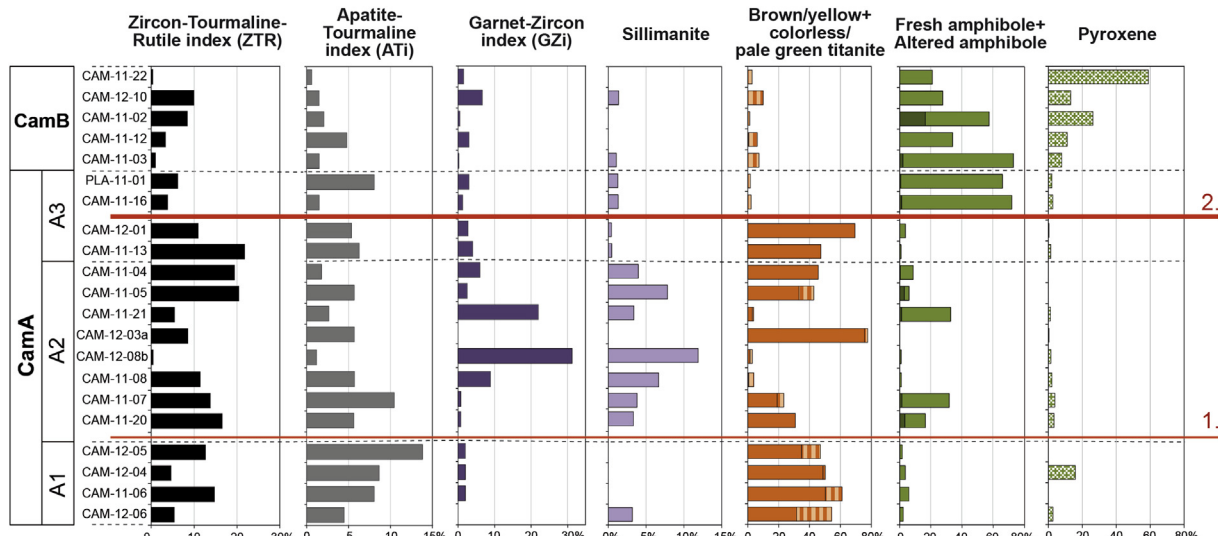


**Fig. 9.** Relevant parameters of the heavy mineral spectra of the Camaná Formation. Positioning of samples within each unit or sub-unit is tentative. Variations in particular heavy minerals support two major shifts in sediment provenance (red lines). ZTR = zircon-tourmaline-titite index, ATI = apatite-tourmaline index, GZi = garnet-zircon index (according to Hubert, 1962; Morton and Hallsworth, 1994). Percentages related to the whole heavy mineral spectra for each sample. Abbreviations are given in Table 2. Location of samples is shown in Fig. 3. (For interpretation of the references to colour in this figure legend, the reader is referred to the web version of this article.)

10%, sample CAM-11-05) (see Fig. 9). Sil, Amp<sub>2</sub>, and Rt are minor constituent, and we want to highlight that the proportions of these heavy minerals are significantly higher in some strata than others (Sil: up to 12%, sample CAM-12-08b; Rt: 14%, sample CAM-11-04). Very minor components are Tur, Pxn, and Amp<sub>1</sub> (less than 10%). The values of the ZTR and the GZi indexes in sediments of A2 and lower A3 are the highest of the Camaná Formation (up to 22% and 35%, respectively) (left side in Fig. 9). The additional input of garnets and sillimanites is considered as the first shift in provenance of the Camaná Formation (lower red line in Fig. 9), and reflects the exhumation of additional source rocks (i.e. the Arequipa Massif, see Section 5.3).

Strata of the upper part of the sub-unit A3 and CamB unit, besides containing a large amount of reworked ash, show a marked change in the mineralogical composition compared to underlying strata of sub-units A2 and lower A3. This is reflected in a drastic increase of Amp<sub>2</sub> (up to 71%, sample CAM-11-16), Pxn (up to 59%, sample CAM-11-22), and Ep (up to 36%, sample CAM-11-12) (Fig. 9). These strata are also featured by dramatic decrease of Ttn<sub>1</sub> (up to 1%, sample CAM-11-12), Grt<sub>1</sub> (up to 5%; rarely 13% e.g. sample CAM-12-10), and absence of sediments with Grt<sub>2</sub>. Additional subordinate components are Amp<sub>1</sub> (up to 2%) and rarely up to 17% (sample CAM-11-02), Ap (up to 11%, sample PLA-11-01), and Ttn<sub>2</sub> (up to 10%, CAM-12-10). Rt, Tur, Zrn, and Sil show very minor concentrations (less than 10%). The values of the ZTR, ATI, and GZi indexes in sediments of the upper part of A3 and CamB are the lowest of the Camaná Formation. The high proportions of pyroxenes, amphiboles, and epidotes of upper A3 and CamB support a second and drastic mineralogical shift (upper red line in Fig. 9).

#### 4.3. Geochemistry of titanite grains

Titanite is present in both the Camaná Formation and the potential source rocks. Due to its relative chemical stability, titanite is expected to record the original crystal chemical composition through time (Morton, 1991; Mange and Maurer, 1992; Ando et al., 2012; von Eynatten and Dunkl, 2012). Titanite can thus be used as

mineral tracer to discriminate sediment provenance by means of geochemical analysis.

##### 4.3.1. Titanites from potential source rocks

In southern Peruvian forearc, parental titanites ( $n = 55$ ) are differentiated according to their color in two types, i.e. (i) Ttn<sub>1</sub> (brown/yellow) (Fig. 8A) and (ii) Ttn<sub>2</sub> (colorless/pale green) (Fig. 8B). We describe the geochemical features of titanites from four potential source rocks, i.e. the San Nicolas Batholith, the Arequipa Massif, the Coastal Batholith, and the Tacaza Group, and constrain their chemical variations by comparing chemical proxies that best reflect the contribution of specific source rock lithologies. Some plots showing these relationships and allow for discrimination of source rocks (Fig. 10). Results of the chemical analysis are listed in the Electronic Appendix.

LA-ICP-MS analyses accomplished on titanites demonstrated that Ttn<sub>1</sub> (which are derived solely from the San Nicolas Batholith, blue symbols in Fig. 10), shows higher proportions of Fe, Al, and Nb + Ta than any Ttn<sub>2</sub> of the remaining potential source rocks. Some chemical proxies are suited for further discriminations among Ttn<sub>2</sub> grains of the Arequipa Massif (brown symbols in Fig. 10), the Coastal Batholith (green symbols in Fig. 10), and the Tacaza Group (yellow symbols in Fig. 10). For instance, Ttn<sub>2</sub> of the Arequipa Massif yield the highest REE concentrations of the group of colorless/pale green titanites (generally 2080–20161 ppm; see Appendix). Ttn<sub>2</sub> of the Coastal Batholith shows on average the highest Al values (from 7430 to 9410 ppm), U values (generally between 166 and 727 ppm) and Nb + Ta concentrations (between 196 and 2545 ppm) of this group, and it shows smaller Fe/Al ratios (between 0.94 and 1.82) than Ttn<sub>2</sub> of Arequipa Massif. Ttn<sub>2</sub> of the Tacaza Group shows the lowest concentrations of Al, REE, and Nb + Ta of both types of titanite, while the values of Fe/Al and Zr/Hf are the highest.

##### 4.3.2. Detrital titanites from the Camaná Formation

According to the division of Alván and von Eynatten (2014) (i.e. CamA and CamB units), detrital titanites ( $n = 158$ ) are displayed as black symbols (CamA unit) and red open symbols (CamB unit) in

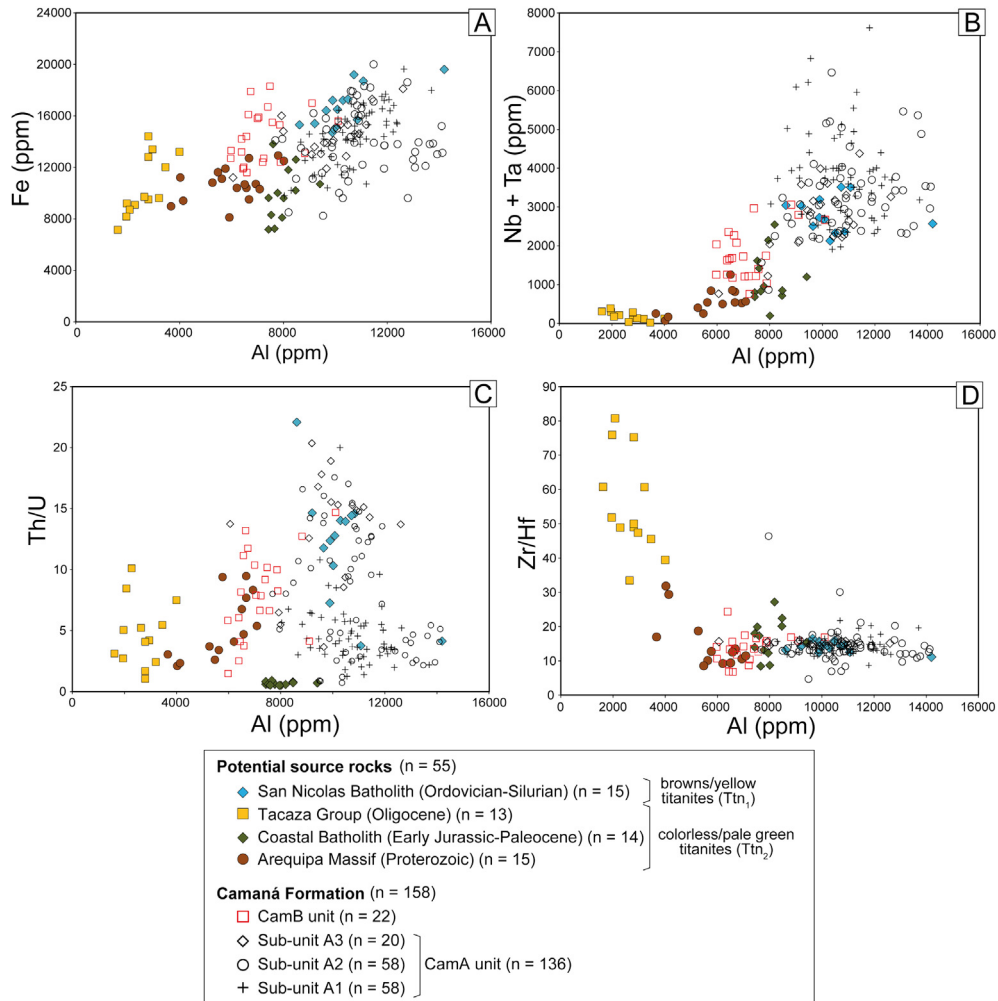


**Fig. 10.** Chemical composition of titanites from four potential source rocks (filled symbols) and the Camaná Formation (open symbols) shown in bivariate variation diagrams. A: Fe (ppm) versus Al (ppm), B: Nb + Ta (ppm) versus Al (ppm), C: Th/U versus Al (ppm), D: Zr/Hf versus Al (ppm). All diagrams show clear differentiation of the potential source rocks. Titanites of CamA (black open symbols) and CamB (red open symbols) are slightly overlapping, they are clearly distinguished by lower Al and (Nb + Ta) content and smaller Th/U range. (For interpretation of the references to colour in this figure legend, the reader is referred to the web version of this article.)

**Fig. 10.** The titanites of the sub-unit A3 correspond mostly to titanites of the lower part of this sub-unit.

The concentrations of Al were crucial to characterize  $Ttn_1$  and  $Ttn_2$  when comparing them to Fe and Nb + Ta concentrations, or Th/U, and Zr/Hf ratios, providing consistent discriminations. In Fig. 10, we observe clear distinctions among titanites of the Camaná Formation (black and brown open symbols reflecting CamA and CamB, respectively). Fe versus Al diagram in Fig. 10A shows that titanites of CamA (black open symbols) overlap entirely the field of the  $Ttn_1$ -bearing rocks of the San Nicolas Batholith. Moreover, minor proportions of titanites of CamA partly overlap with the fields of the Arequipa Massif and the Coastal Batholith ( $Ttn_2$ -bearing rocks). Conversely, titanites of CamB unit (red open symbols) partly overlie the brown and green symbols that represent the Arequipa Massif and the Coastal Batholith, respectively. Although a very minor overlap of titanites from CamA and CamB is observed, we note a generally very well defined distinction among them. Scattering patterns of titanites of CamA and CamB in Fig. 10A are very similar to scattering in Fig. 10B, C, and D. Overall, we state that  $Ttn_1$  is typical for sediments of CamA unit, while  $Ttn_2$  is typically observed in sediments of CamB unit. Remarkably, any titanite with similar chemical properties to those of the Tacaza Group ( $Ttn_1$  in yellow symbols) is lacking in the detrital minerals.

## 5. Discussion

### 5.1. The youngest zircon U–Pb age components: chronostratigraphic framework of the Camaná Formation

We use the youngest zircon U–Pb age components instead of the youngest U–Pb single-grain ages to define the sedimentation time because they offer a statistically meaningful way for determining the maximum age of deposition (von Eynatten and Dunkl, 2012). The results of the U–Pb geochronological dating of volcanogenic zircons within the CamA unit (sub-units A2 and A3) yield ages between ~23 and ~14 Ma (Table 1 and Fig. 4) resembling the Early Miocene to early Middle Miocene. We consider these ages as relatively close to the stratigraphic age because zircon U–Pb ages of volcanic products that are derived from active volcanic setting closely resemble depositional ages (e.g. Bowring and Schmitz, 2003; von Eynatten and Dunkl, 2012). The sedimentation time suggested for these sub-units is at least ~9 My. Furthermore, sub-unit A2 ranges in age approximately 3 My duration of deposition (Aquitanian) (see position of ages in Fig. 2).

The sedimentary facies of the Camaná Formation frequently show reworked ashes derived from some of the intermittent pyroclastic emissions of the ~30 to 3 Ma volcanism in southern Peru

and northern Chile. However, there are no evidence of volcanism (e.g. ~30–24 Ma Tacaza volcanic arc or younger) within sediments of the basal part of the CamA unit (sub-unit A1) and thus no Cenozoic zircon or titanite U–Pb ages. We affirm that strata of sub-unit A1 are older than Miocene, based on stratigraphic relations with the overlying ~23–14 Ma tuff-bearing layers and paleontology (Late Oligocene fossil shark teeth in La Mina, Camaná, [Apolín, 2001](#)) (pink area in Fig. 11B). This possibility is further supported by stratigraphic correlations with ~30–25 strata of the contiguous Moquegua Group (sub-unit Moquegua C1 or “MoqC1” of [Decou et al., 2011](#)), where the argument is based on the relative abundance of pyroxenes and epidotes (see Section 5.4). Accordingly, the inferred age of the sub-unit A1 is most likely Late Oligocene.

Sedimentation of CamB unit consists of fluvial conglomerates with alternations of reworked ash. The ages assigned to CamB are late Middle to Late Miocene (between ~12 and ~7 Ma, Table 1 and Fig. 4F to G), and because the topmost part remains undated, it may extends to Pliocene. The volcanic products within the deposits of CamB are closely consistent to the ~10–3 Ma Lower Barroso volcanic arc (e.g. [Mamani et al., 2010](#)). However, younger age components of 8.7, 9.1, and 9.8 Ma were obtained using algorithms different to *Tuffzirc*. These ages, nonetheless, may suggest that the onset of CamB deposition would have begun relatively later, and can be related to a rapid cooling and onset of valley incision occurred at ~9 Ma in Western Cordillera and western Altiplano (~9 Ma, apatite [U–Th]/He data, [Schildgen et al., 2007](#)). In terms of sediment provenance, these ages still reflect the activity of the early stage of the Lower Barroso volcanic arc ([Mamani et al., 2010](#)). Overall, the stratigraphic ages of the Camaná Formation are Late Oligocene to Late Miocene or Pliocene. Several ages similar to the ~24–10 Ma Huayllillas and the ~10–3 Ma Lower Barroso volcanism were broadly documented in southern Peru and northern Chile (e.g. in the Western Cordillera of the provinces of Moquegua and Tacna in southern Peru, in northernmost Chile, and minor proportions in the Altiplano of Arequipa ([Quang et al., 2005; Mamani et al., 2010](#); and references therein).

## 5.2. The significance of brown/yellow and colorless/pale green titanites

Brown/yellow titane ( $\text{Ttn}_1$ ) derives exclusively from granites of the San Nicolas Batholith (Fig. 8A), while colorless/pale green titanite ( $\text{Ttn}_2$ ) occurs in gneisses of the Arequipa Massif and in diorites of the Coastal Batholith, the Toquepala Group, and the Tacaza Group (Fig. 8B). [Frost et al. \(2000\)](#) and [Aleinikoff et al. \(2002\)](#) proposed to differentiate types of titanite according to the color (brown/yellow and colorless/pale green). They suggested that brown/yellow titanites (our  $\text{Ttn}_1$ ) show higher Fe, U, Ce, Nb, and REEs values, also higher Th/U, and Fe/Al ratios, and lower Al and  $\text{Al}_2\text{O}_3$  values than colorless/pale green titanites (our  $\text{Ttn}_2$ ). According to [Frost et al. \(2000\)](#) and [Aleinikoff et al. \(2002\)](#), titanites rich in Al that are formed in metamorphic rocks tend to have a lower refraction index and lower birefringence than those that have less Al content (igneous rocks), and darker titanites show higher content of Fe than titanites with light colors.

Such statements agree with the statements of these authors, where titanites of the Tacaza Group ( $\text{Ttn}_2$ ) show the highest ratios of Fe/Al. However, titanites of the San Nicolas Batholith ( $\text{Ttn}_1$ ) still show higher Al, Fe, and lower U and Fe/Al values than most of  $\text{Ttn}_2$ .  $\text{Ttn}_1$  shows higher refraction index and birefringence than  $\text{Ttn}_2$  (Fig. 8). This may be explained in a possible later assimilation of REEs for the San Nicolas Batholith from the REE-rich Arequipa Massif. This study demonstrates moreover that  $\text{Ttn}_2$  also occurs in igneous rocks (e.g. diorites of the Coastal Batholith), and not only in metamorphic rocks.

## 5.3. Provenance model of the Camaná Formation

We present a sedimentary provenance model based on integrating information from zircon and titanite U–Pb geochronology (Section 4.1), analyses of heavy mineral spectra in sediments of the Camaná Formation and source rocks (Section 4.2), and chemical analysis on parental and detrital titanites (Section 4.3). Within the

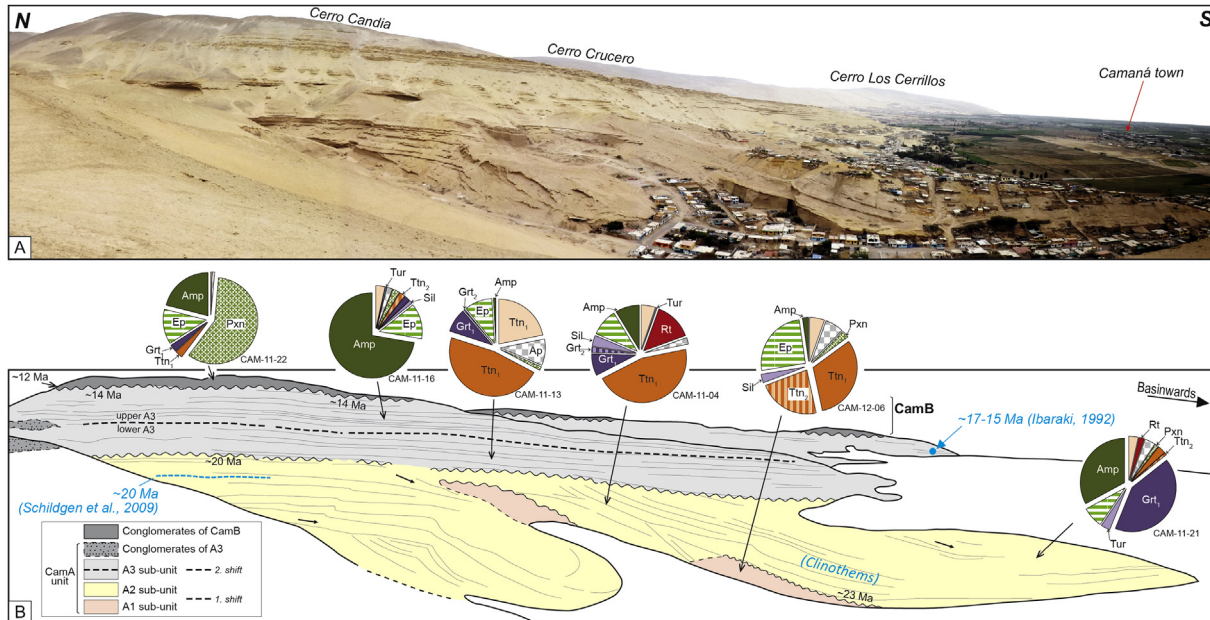


**Fig. 11.** In A: Representative exposures of the Camaná Formation (La Mina Section) (modified from [Alván and von Eynatten, 2014](#)). In B: Representative heavy minerals in the Camaná Formation. Ma ages in black words are extracted from Table 1, and ages in blue are previous works. See abbreviations of heavy minerals in Table 2. (For interpretation of the references to colour in this figure legend, the reader is referred to the web version of this article.)

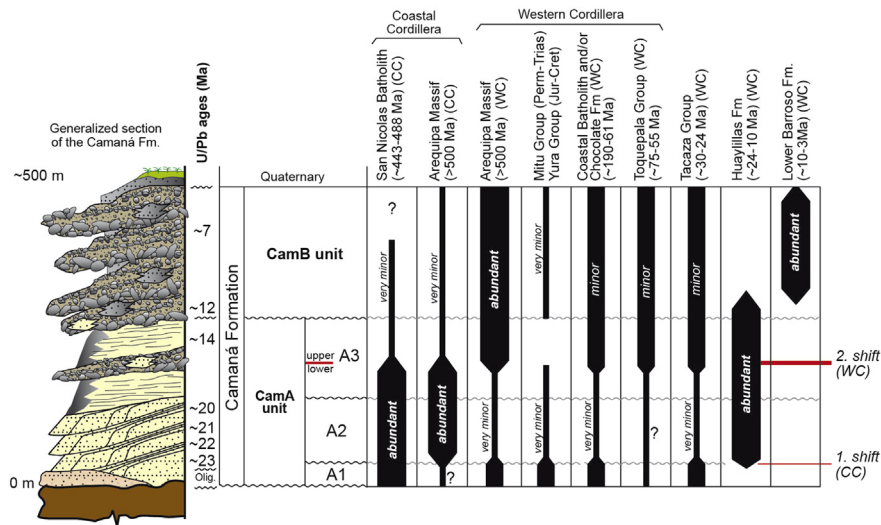


**Fig. 12.** Provenance model is based on heavy mineral assemblages, U–Pb geochronology on zircons and titanites, and LA-ICP-MS analysis on titanites. The thickness of the black bars refers to relative abundance of each source lithology within each sub-unit. Stratigraphic framework is proposed by Alván and von Eynatten (2014). WC = Western Cordillera, CC = Coastal Cordillera.

Camaná Formation, we observe three different heavy mineral spectra grouped as (i) A1, (ii) A2 and lower A3, and (iii) upper A3 and CamB (Figs. 7 and 9). Consequently, we define two major shifts in sediment provenance within the Camaná Formation (Fig. 12).

The lowermost part of CamA unit (sub-unit A1) shows provenance mostly from the San Nicolas Batholith (Coastal Cordillera). This statement is inferred on the predominance of Ordovician and Silurian zircon and titanite U–Pb ages (see Fig. 5A). Chemical composition of detrital titanites supports that statement (Fig. 10). A minor contribution from the Arequipa Massif, the Coastal Batholith, the Tacaza Group, and the Mitu and/or Yura Groups from the hinterland Western Cordillera is also inferred on the presence of some characteristic heavy minerals, such as epidotes, pyroxenes, and colorless/pale green titanites. Accordingly, we interpret that during the Late Oligocene age only the San Nicolas Batholith was exposed to denudation, being the main provenance of this sub-unit. Minor source rocks are the Arequipa Massif (Western Cordillera), the Mitu and/or Yura Groups, the Coastal Batholith, and the Tacaza Group.

During the Early to Middle Miocene age, the Arequipa Massif of the Coastal Cordillera became additional source lithology for sub-units A2 and the lower part of A3, besides the San Nicolas Batholith (Fig. 5B to E). This is inferred on the striking contribution of garnets and sillimanites that are derived from the Arequipa Massif (see Fig. 6). Evidences of the widespread volcanism of the ~24–10 Ma Huayllillas volcanic arc are interspersed in these strata, and also form main source lithology. This input represents a “first” (although slight) shift in sediment provenance observed in the Camaná Formation (lower red line in Fig. 12), and may reflect continuation of uplifting of the Coastal Cordillera (see Section 5.5). Additionally, subordinate proportions of pyroxenes and amphiboles resemble provenance of the amphibole-rich Coastal Batholith (and/or Arequipa Massif of the Western Cordillera, Fig. 7) and pyroxene-bearing Tacaza Group, and a minor occurrence of rutiles might suggest provenance of either the Mitu and/or Yura Groups. This statement is also supported by minor proportions of zircon U–Pb single-grain ages of ~150 and ~270 Ma.

Sediments of upper A3 and CamB differ largely in heavy mineral composition from the sub-units A1, A2, and lower A3. According to our zircon U–Pb age components (~14–~7 Ma) these sediments are predominantly derived from the products of the final stage of the ~24–10 Ma Huayllillas volcanism (mainly as pyroclasts and

reworked ashes) and the ~10–3 Ma Lower Barroso volcanic arc (pyroclasts, rhyolites, and andesites). Additionally, the occurrence of sediments derived of the Arequipa Massif of the Western Cordillera is interpreted on the base of abundant zircon U–Pb single-grain ages between ~1870 and ~950 Ma (Fig. 5F). Titanite chemistry supports this statement, reflecting composition similar to the Arequipa Massif (red open symbols in Fig. 10). Minor proportions of zircons single-grain U–Pb ages between ~240 and ~65 Ma, ~30 Ma, and titanite individual ages between ~85 Ma and ~34 Ma (blue lines in Fig. 4F) resembles the ages of the Coastal Batholith (and/or the Chocolate Formation), and the Tacaza Group.

There are no chemical signals of titanites derived from the Tacaza Group in these strata as observed in Fig. 10. Despite relative resistance of heavy minerals e.g. epidotes, staurolites, and titanites, they may disappear by weathering and/or burial dissolution (Morton and Hallsworth, 1999; Ando et al., 2012). In the case of the Camaná Formation, we consider that the burial depth of the Camaná Formation is shallow, and we attribute the lack of  $Ttn_2$  derived from the Tacaza Group to a progressive corrosion triggered mostly by long transport and traction (>100 km away from Camaná, see site “a” in Fig. 1C). Heavy minerals i.e. pyroxenes and epidotes feature the composition of the uppermost CamA and CamB unit (samples CAM-11-22 and CAM-11-16 in Fig. 11A), and they are only observed in diorites of the Tacaza Group. According to Freise (1931), Thiel (1940), and Dietz (1973), titanite is more resistant to mechanical abrasion than pyroxene. The reason of having abundant pyroxenes and absence of colorless/pale green titanites in these strata may be due to their differences in abundance, as seen in sample TAZ-00-03 in Fig. 6. Consequently, we can also consider the Tacaza Group as minor source rock. The contribution of rutiles and tourmalines derived from the Yura and/or Mitu Groups and the San Nicolas Batholith are very minor, and they are also considered as minor source rocks.

Overall, main source rocks for upper A3 and CamB are the Barroso volcanic arc and the Arequipa Massif of the Western Cordillera. Minor source rocks are the Tacaza Group, the Toquepala Group, the Coastal Batholith, the Mitu and/or Yura Groups, the Arequipa Massif of the Coastal Cordillera, and the San Nicolas Batholith. Collectively, sediments of the upper part of sub-unit A3 and CamB unit represent a second and drastic shift in the sediment provenance of the Camaná Formation since ~14 Ma. We consider this shift as

intimately related to a pulse of tectonic uplift in the Western Cordillera (see Section 5.5).

The onset of the second major shift in provenance is not precisely consistent with the onset of CamB deposition; it is located in the upper part of the sub-unit A3 of CamA (Figs. 8 and 9). Nonetheless, it is largely consistent with local deposition of conglomerates (with pebbles derived from the Western Cordillera) that occurred first time in the upper part of the sub-unit A3 (cf. Alván and von Eynatten, 2014) (see upper red line in Fig. 12).

#### 5.4. Correlation with the Moquegua Group

Decou et al. (2011) noted a significant change in mineral composition and sedimentary facies within the MoqC unit, allowing a tentative sub-division into the pyroclastic-poor MoqC1 (lowermost MoqC) and the tuff-rich MoqC2 sub-units (uppermost MoqC). According to these authors, the most abundant heavy minerals in this unit are pyroxenes, epidotes, and amphiboles (Table 3). Using zircon U–Pb geochronology, electron microprobe analysis (EMPA) on amphiboles, and zircon fission track data, Decou (2011) suggested moreover that sediments of MoqC1 are derived predominantly from magmatic rocks the ~30–25 Ma Tacaza Group. Sub-unit MoqC2 reflects much stronger volcanic input and a predominant provenance from the ~24–10 Ma Huayllillas Formation.

The first chronostratigraphic equivalence of the Moquegua Group and the Camaná Formation is between CamA and MoqC units, with sub-unit A1 corresponding to ~30–25 sub-unit MoqC1 of Decou et al. (2011). This statement is based on the stratigraphic position of the sub-unit A1 under the dated ~23–14 Ma strata of sub-unit A2 and A3 of the Camaná Formation. Although main source rock of the sub-unit A1 is the San Nicolas Batholith, with additional heavy minerals similar to those observed in sediments of MoqC1 (i.e. pyroxenes of the Tacaza Group). (Table 3) Within the sub-units A2 and A3 of the Camaná Formation, the striking abundance of reworked ashes dated at ~23 to ~14 Ma, make them

roughly equivalent to the ~25 to 15–10 Ma sub-unit MoqC2 of Decou et al. (2011). These ages are consistent with the emplacement of the widespread ignimbrite volcanism in the region (Huayllillas and Oxaya, Wörner et al., 2002; Thouret et al., 2007; Mamani et al., 2010).

The next equivalence is proposed between CamB and MoqD units. The depositional age of MoqD is roughly constrained as 15–10 to ~4 Ma (Sempere et al., 2004; Decou et al., 2011). The age of CamB is well-defined between ~12 and ~7 Ma, and may be even extend to the Pliocene). A correlation between CamB and MoqD may suggest that sedimentation of both started at ~12 Ma. This age is slightly older than the onset of the Lower Barroso volcanism, the products of which are widespread within conglomerates of CamB. A predominance of pyroxenes and amphiboles in both MoqD and CamB illustrates as well additional common provenance from the Tacaza Group, the Huayllillas Formation, and the Toquepala Group.

#### 5.5. Geodynamic evolution of the southern Peruvian forearc

Based on thermochronological data (apatite [U–Th]/He data), Wipf (2006) suggested that Proterozoic rocks of the Coastal Cordillera in southern Peru have experienced slow cooling until Late Cretaceous, followed by a period of geodynamic quiescence until Late Miocene. Conversely, Oncken et al. (2006) suggested that this part of the Central Andes experienced more or less continuous shortening and uplift since at least Late Eocene. We support the latter statement and place further constraints on the geodynamic history of this part of the Central Andes by our provenance study.

We have inferred the age of the sub-unit A1 as Late Oligocene; accordingly, we suggest that the uplift and exhumation of the Coastal Cordillera might have occurred since that time.

The onset of deposition of the sub-unit A1 is roughly consistent with some remarkable points. These include (i) a striking change in sediment provenance estimated at ~30 Ma at the latest within the Moquegua Group (Decou et al., 2013), (ii) onset of major phase of

**Table 3**  
Summary of heavy mineral spectra of potential source rocks and the Camaná Formation and the upper part of the Moquegua Group (MoqC and MoqD units). For heavy mineral abbreviations see Table 2. Symbols: xxx = abundant (~75–25%), xx = common (~25–15%), x = present (~15–1%), o = absent. Colored boxes highlight occurrences of key minerals for provenance analysis. (\*) indicates samples analyzed firstly by Decou et al. (2011) and later refined in this study.

Lithology		Zrn	Tur	Ap	Rt	Sil	Grt1	Grt2	Ttn1	Ttn2	Pxn	Ep	Amp1	Amp2
Potential source rocks	Lower Barroso arc(10-3 Ma) ignimbrite (*)	o	o	o	o	o	o	o	o	o	o	o	xx	o
	Lower Barroso arc(10-3 Ma) andesites, dacites (*)	o	o	x	o	o	o	o	o	o	xxx	o	o	o
	Huayllillas arc (24-10 Ma) ignimbrites (*)	x-xx	o	x-xx	o-x	o	o	o	o	o	o	o	xx-xxx	o
	Huayllillas arc (24-10 Ma) andesites (*)	o	o	x	o	o	o	o	o	o	xxx	o	o	o
	Tacaza arc (30-24 Ma) andesites (*)	o	o	xx	o	o	o	o	o	o	xxx	o	o	o
	Tacaza arc (30-24 Ma) diorites	o	o	o	o-x	o	o	o	o	o	x	xx-xxx	xxx	o
	Anta arc (45-30 Ma) andesites, diorites (*)	x	o	o-xx	o	o	o	o	o	o	xxx	o	o-x	o
	Toquepala arc (91-45) rhyolite	x	o	o	o	o	o	o	o	o	o	o	o	xx
	Toquepala arc (91-45) plutonics	o-x	o	x-xx	o	o	o	o	o	o	o	o	o	xx-xxx
	Coastal Batholith (190-60) plutonics	o-x	o	x	o	o	o	o	o	o	x	x	x	xxx
	Yura Group (Jurasic-Cretaceous)	xxx	xx	x	xx-xxx	o	o	o	o	o	o-x	x	o	o-x
	Mitu Group (Permian-Triassic)	xxx	xx	x	xx-xxx	o	x	o	o	o	o-x	x	o	o-x
	San Nicolas Batholith (Silurian-Ordovician)	x	o	x	o	o	o-x	o	xxx	o	o	x	o	x
	Arequipa Massif (Proterozoic) gneiss	xx	o	x-xx	o-x	o	o	x-xx	o	x	o	xx-xxx	o	xx-xxx
	Arequipa Massif (Proterozoic) granulites	xx	x	o-x	o	x	xxx	o	o	x	x	x	o	x
	Arequipa Massif (Proterozoic) amphibolites (*)	xx	o	xx	o	o	o	o	o	o	o	o	o	xx-xxx
Moquegua Group		o-x	o	x	o-x	x	o	xx	o	x	xxx	xxx	x-xx	xx-xxx
MoqC2 (*)		xx	o-x	x	o-x	o	o-x	o-x	o	o-x	xx-xxx	xx-xxx	x-xx	o-x
MoqC1 (*)		x-xx	o	xx	x	o	o-x	o-xxx	o	o-x	x-xxx	xx-xxx	o-x	x-xx
Camaná Formation	CamB	x	o-x	x	o-x	o-x	x	o	o	x	xxx	xxx	xx	xxx
	upper A3	x	o-x	x	o	x	x	o	o	x	o-x	x	xx	xxx
	lower A3	xx	o-x	x	o	o-x	x	o	xxx	o	o-x	x	o	o-x
	A2	xx	o-x	x	xx	x	x-xxx	x-xxx	xxx	o-x	o-x	xx	o-x	x-xxx
	A1	x	o-x	xx	o-x	o-x	o-x	o	xxx	xx	xx	xx	o	x

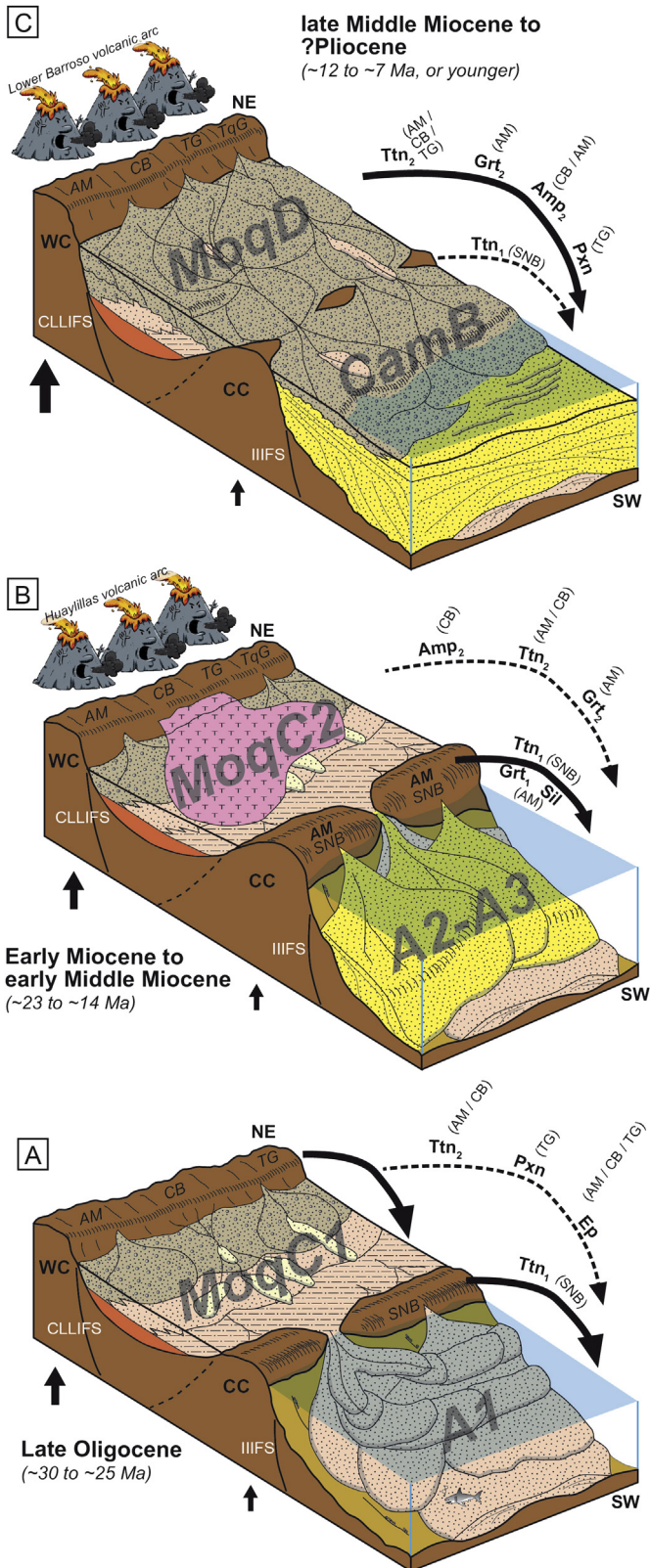


**Fig. 13.** Evolutionary model of the Camaná Formation in Camaná. Not to scale. A: Deposition of A1 of CamA unit. A1 consists of mouth bars and distributary channels (Late Oligocene, or likely older). B: Deposition of A2 + A3 of CamA. A2 + A3 consist of prograding clinothems and onlapping deposits, respectively (Early Miocene to early Middle Miocene). C: Deposition of CamB. CamB unit consists of fluvial conglomerates (late middle Miocene to Pliocene). Abbreviations: AM = Arequipa Massif, CB = Coastal Batholith, TG = Tacaza Group, TqG = Toquepala Group, WC = Western Cordillera,

shortening and thickening of the upper crust during flat-slab subduction (~30 Ma, [Kay, 2005](#); [Haschke et al., 2006](#)), and (iii) waning of tectonic rotations along the south Peru margin ([Roperch et al., 2006](#)). Such important geodynamic events are reflected in the composition of the relevant sedimentary units or sub-units of the Camaná Formation. In Early Miocene, the onset of widespread volcanism i.e. Huayllillas marks the beginning of renewed steeping of the slab and westward arc migration ([Mamani et al., 2010](#)). We relate this setting to deposition of sub-units A2 and A3. Uplift of the Coastal Cordillera was accompanied by simultaneous uplift of the Western Cordillera. From ~25 Ma until present day, uplift of the western flank of the Western Cordillera is estimated at 2.3–1.8 km ([Thouret et al., 2007](#); [Schildgen et al., 2009](#)) and strongly influenced the deposition of MoqC and MoqD units ([Decou et al., 2013](#)).

Despite uplift of the Coastal Cordillera and separation of the Camaná and the Moquegua Basins since at least ~30 Ma (Fig. 1B), sediments derived from the Western Cordillera are present in minor proportions in deposits of the Camaná Formation, and suggesting connectivity between both of the basins.

At ca. 12 to 10 Ma, low convergence rates and obliquity in the Central Andes ([Pardo-Casas and Molnar, 1987](#); [Somoza, 1998](#)) mark the onset of the widespread volcanism of the Lower Barroso ([Mamani et al., 2010](#)). This is consistent with the onset of well-documented Late Miocene valley incision of the hinterland (Western Cordillera), which is inferred to reflect Late Miocene rapid uplift of the Western Cordillera (e.g. [Gregory-Wodzicki, 2000](#); [Schildgen et al., 2007, 2009](#); [Thouret et al., 2002, 2007](#); [Garzione et al., 2008](#)). The onset of Lower Barroso volcanism and valley incision is also consistent with a marked change in depositional style and facies in the Moquegua and Camaná basins i.e. onset of MoqD and CamB units, respectively. This change coincides with a major shift in sediment provenance of the Camaná Formation (upper red line in Fig. 12) which now indicates major provenance from the Western Cordillera. Consequently, if sediments similar to the MoqD unit extended into the Camaná Basin (as CamB unit), it suggests that the uplift rate of the Coastal Cordillera decreased, and the influence of the Coastal Cordillera on sedimentation in the Camaná Basin strongly diminished.

A rough estimation of the uplift of the Coastal Cordillera since ~12 Ma is based on the fact that the basal strata of CamB unit were deposited very close to sea-level ([Alván and von Eynatten, 2014](#)). At present day, these deposits are located at ~500 m above sea level. Consequently, uplift of the Coastal Cordillera since ~12 Ma is about 0.5 km. The uplift of the Western Cordillera is inferred to be much higher and has triggered incision of 2.4–3 km in the deepest reaches (Cotahuasi Valley) starting after ~11 Ma ([Schildgen et al., 2009](#)). Therefore, these estimates support that uplift of the Western Cordillera over-exceeded uplift of the Coastal Cordillera since about 14–12 Ma.

Summarizing, our statements suggest that since about Late Oligocene (Chattian) to Middle Miocene (Langhian) the Western and Coastal Cordilleras have experimented roughly similar uplift (Fig. 13A and B), while during Middle Miocene (Serravalian) to Pliocene the uplift of the Western Cordillera clearly exceeded the uplift of the Coastal Cordillera (Fig. 13C).

CC = Coastal Cordillera. Heavy minerals: Zrn = zircon, Tur = tourmaline, Rt = rutile, Ap = apatite, Pxn = pyroxene, Ttn<sub>1</sub> = brown/yellow titanite, Ttn<sub>2</sub> = colorless/pale green titanite, Grt<sub>1</sub> = pink garnet, Grt<sub>2</sub> = colorless/pale green garnet, Sil = sillimanite, Ep = epidote, Amp<sub>1</sub> = fresh amphibole, and Amp<sub>2</sub> = altered amphibole. Black continuous arrows indicate main provenance. Black dotted arrows indicate minor provenance. (For interpretation of the references to colour in this figure legend, the reader is referred to the web version of this article.)

## 6. Conclusions

1. U–Pb geochronology on volcanic zircons and titanites allows for defining the sedimentation ages of the Camaná Formation. The CamA unit of the Camaná Formation is considered as chrono-logic equivalent to the MoqC unit of the Moquegua Group. Further correlations are proposed among their respective sub-units. Deposition of sub-unit A1 can be assigned to the Late Oligocene based on biostratigraphic evidence as well as litho-stratigraphic and petrographic correlations with the ~30–25 Ma MoqC1 sub-unit of the Moquegua Group. The youngest zircon U–Pb age components are  $23.0 \pm 0.4$  Ma and  $21.7 \pm 1.3$  Ma at the base of sub-unit A2,  $20.0 \pm 0.6$  Ma at the top of the sub-unit A2, and  $13.6 \pm 0.4$  Ma at the top of sub-unit A3. These ages closely resemble the depositional age of the tuff and ignimbrite-rich MoqC2 sub-unit according to Decou et al. (2011). Sub-units A2 and A3 of CamA thus span the Early Miocene (Aquitanian) to Middle Miocene (Langhian) (~14 My). The CamB unit is dated at  $12.4 \pm 0.3$  Ma at the base, and  $7.5 \pm 0.4$  Ma near the presently-exposed top by considering the youngest zircon U–Pb age components derived of reworked ashes. Sedimentation of CamB unit may have continued after ~7 Ma. Hence, sedimentation of CamB unit is assigned to the Middle Miocene (Serravalian) to Late Miocene (Messinian), and may extend to the Pliocene. This makes CamB unit chronostratigraphically equivalent to the MoqD unit of Moquegua Group. Given further similarities in facies, conglomerate clast composition and heavy mineral analysis, we conclude that deposition of MoqD unit extended into the Camaná Basin as CamB unit (here termed CamB unit).
2. The Camaná Basin fill was largely controlled by uplift of the Coastal Cordillera and the Western Cordillera, which occurred differentially with respect to time and rates of uplift. This conclusion is mainly based on the proposed provenance model for the sediments forming the CamA and CamB units of the Camaná Formation (Figs. 12 and 13). The heavy mineral spectra of the Camaná Formation reveal that sediments of CamA unit are predominantly derived from the San Nicolas Batholith of the Coastal Cordillera. The addition of sediments derived from the Arequipa Massif of the Coastal Cordillera and contribution of the widespread ~24–10 Ma-old Huayllillas volcanism to deposition of sub-units A2 and lower A3 signals a first, although slight, shift in provenance (lower red line in Fig. 12). Within CamA unit, minor proportions of heavy minerals derived from rocks forming the Western Cordillera (i.e. Arequipa Massif of the Western Cordillera, Coastal Batholith, and Tacaza Group) suggest minor sediment contribution from the Western Cordillera. Sediments of the uppermost part of sub-unit A3 and CamB unit are largely derived from the latest stage of the ~24–10 Ma-old Huayllillas volcanism, the widespread ~10–3 Ma-old Lower Barroso volcanism, and the Arequipa Massif (of the Western Cordillera). This second shift in provenance is very prominent in the Camaná Formation (upper red line in Fig. 12). It separates two main geodynamic scenarios for the southern Peruvian forearc: (i) Since ~30 to ~14 Ma, the Coastal Cordillera was uplifted and has controlled deposition of CamA unit. During this uplift, material derived from the Arequipa Massif of the Coastal Cordillera was progressively added to the dominant sources of the San Nicolas Batholith. Since ~24 Ma volcanic material was also added (Huayllillas). Uplift and exhumation occurred most likely by means of transcurrent motions along the Ica-Ilo-Islay Faults System (Fig. 13B). (ii) From ~14 to 12 Ma to <7 Ma (possibly until the Early Pliocene), uplift of the Western Cordillera strongly exceeded uplift of the Coastal Cordillera. Consequently, sedimentation of the uppermost sub-unit A3 and CamB unit are strongly

controlled by uplift of the Western Cordillera (Fig. 13C). The timing of accelerated uplift in the Western Cordillera at ~14–12 Ma is corroborated by the slightly later onset of the major incision in the Western Cordillera and the forearc, as demonstrated by Thouret et al. (2007), Schildgen et al. (2007, 2009), Garzione et al. (2008), and the onset of the Lower Barroso volcanism at ~10 Ma (Mamani et al., 2010).

## Acknowledgments

Financial support by the Deutscher Akademischer Austauschdienst (DAAD, Referat 416/PKZ A/09/98944) provided to AA to carry out this research is gratefully acknowledged. We thank Taylor Schildgen (Potsdam) for numerous critical remarks on an earlier version of the manuscript, and Mirian Mamani (Lima) for valuable discussions. Detailed and thoughtful comments by Luca Caracciolo (Calabria) and an anonymous reviewer helped to improve the manuscript. Supplementary data associated with this manuscript is available in the online version.

## Appendix A. Supplementary data

Supplementary data related to this article can be found at <http://dx.doi.org/10.1016/j.jsames.2015.02.008>.

## References

- Acosta, H., Alván, A., Rodríguez, J., 2010a. Actividad tectónica del Sistema de Fallas Cincha-LLuta-Incapuquio durante la evolución de la cuenca Arequipa en el Jurásico. In: XV Congreso Peruano de Geología, Cusco. Sociedad Geológica del Perú, Resúmenes Extendidos, pp. 742–745.
- Acosta, H., Oviedo, M., Rodríguez, J., Alván, A., 2010b. Mapa geológico y perfiles del Cuadrángulo de La Yesera (33q-I, 33q-II, 33q-III y 33q-IV). Escala 1:50 000 (4 mapas). INGEMMET. Dirección de Geología Regional, Lima, Perú.
- Acosta, H., Oviedo, M., Rodríguez, J., Alván, A., 2010c. Mapa geológico y perfiles del Cuadrángulo de Ocoña (33p-I, 33p-II, 33p-III y 33p-IV). Escala 1:50 000 (4 mapas). INGEMMET. Dirección de Geología Regional, Lima, Perú.
- Aleinikoff, J.N., Moore, T.E., Walter, M., Nokleberg, W.J., 1993. U–Pb ages of zircon, monazite, and sphene from Devonian metagranites and metafelsites central Brooks Range, Alaska. U. S. Geol. Surv. Bull. B 2068, 59–70.
- Aleinikoff, J.N., Wintsch, R.P., Fanning, C.M., Dorais, M.J., 2002. U–Pb geochronology of zircon and polygenetic titanite from the Glastonbury complex, Connecticut, USA: an integrated SEM, EMPA, TIMS, and SHRIMP study. Chem. Geol. 188, 125–147.
- Allmendinger, R.W., Jordan, T.E., Kay, S.M., Isacks, B.L., 1997. The evolution of the Altiplano-Puna plateau of the Central Andes. Annu. Rev. Earth Planet. Sci. 25, 139–174.
- Alván, A., von Eynatten, H., 2014. Sedimentary facies and stratigraphic architecture in coarse-grained deltas: anatomy of the cenozoic Camaná formation, Southern Peru ( $16^{\circ}25'S$  to  $17^{\circ}15'S$ ). J. South Am. Earth Sci. 54, 82–108.
- Ando, S., Garzanti, E., Padoan, M., Limonta, M., 2012. Corrosion of heavy minerals during weathering and diagenesis: a catalogue for optical analysis. Sediment. Geol. 280, 165–178.
- Apolín, J., 2001. *Isurus oxyrinchus* RAFINESQUE, 1810 “Mako de aletas cortas” como posible ancestro de *Carcharodon carcharias* (LINNAEUS, 1758) “Tiburón blanco” (Chondrichtyes: Lamnidae). Tesis de Ciencias Biológicas. Universidad Nacional Mayor de San Marcos, Lima, Perú, p. 133.
- Bellido, E., 1969. Lima, Perú. Boletín No. Sinopsis de la geología del Perú. Boletín del Servicio de Geología y Minería. Dirección General de Minería (INGEMMET), vol. 22, p. 54.
- Bellido, E., Narváez, S., 1960. Geología del Cuadrángulo de Atico, Hoja 33-o. Boletín No. 2, Serie A. In: Comisión de la Carta Geológica Nacional (INGEMMET), Lima, Perú, p. 59.
- Benavides, V., 1962. Estratigrafía Pre-terciaria de la región de Arequipa. Boletín de la Sociedad Geológica del Perú. In: II Congreso Nacional de Geología (Tomo 38), pp. 5–63.
- Boily, M., Brooks, C., Ludden, J.N., 1989. Chemical and isotopic evolution of the Coastal Batholith of southern Peru. J. Geophys. Res. 94, 483–498.
- Bowring, S.A., Schmitz, M.D., 2003. High-precision U–Pb zircon geochronology and the stratigraphic record. Rev. Mineral. Geochem. 53 (1), 305–326.
- Carlotto, V., Quispe, J., Acosta, H., Rodríguez, R., Romero, D., Cerpa, L., Mamani, M., Díaz-Martínez, E., Navarro, P., Jaimes, F., Velarde, Lu, S., Cueva, E., 2009. Dominios Geotectónicos y Metalogénesis del Perú. Bol. la Soc. Geol. del Perú 103, 1–89.
- Cherniak, D.J., 1993. Lead diffusion in titanite and preliminary results on the effects of radiation damage on Pb transport. Chem. Geol. 110, 177–194.

- Cherniak, D.J., Watson, E.B., 2000. Pb diffusion in zircon. *Chem. Geol.* 172, 5–24.
- Chew, D.M., Magna, T., Kirkland, C.L., Miskovic, A., Cardona, A., Spikings, R., Schaltegger, U., 2008. Detrital zircon fingerprint of the Proto-Andes: evidence for a Neoproterozoic active margin? *Precambrian Res.* 167, 186–200.
- Cobbing, E.J., Pitcher, W.S., 1972. The Coastal Batholith of Central Peru. *J. Geol. Soc.* 128, 421–454.
- Cobbing, E.J., Ozard, J.M., Snelling, N.J., 1977. Reconnaissance geochronology of the crystalline basement rocks of the Coastal Cordillera of southern Peru. *Bull. Geol. Soc. Am.* 88 (2), 241.
- Colella, A., 1988. Fault-controlled marine Gilbert-type fan deltas. *Geology* 16, 1031–1034.
- Decou, A., 2011. Provenance Model of Cenozoic Siliciclastic Sediments from the Western Central Andes (16–21°S): Implications for Eocene to Miocene Evolution of the Andes. *Mathematisch-Naturwissenschaftlichen Fakultäten. Georg-August Universität Göttingen, Göttingen*, p. 125.
- Decou, A., von Eynatten, H., Mamani, M., Sempere, T., Wörner, G., 2011. Cenozoic forearc basin sediments in Southern Peru (15–18°S): stratigraphic and heavy mineral constraints for Eocene to Miocene evolution of the Central Andes. *Sediment. Geol.* 237, 55–72.
- Decou, A., von Eynatten, H., Dunkl, I., Wörner, G., 2013. Late Eocene to Early Miocene Andean uplift inferred from detrital zircon fission track and U-Pb dating of Cenozoic forearc sediments (15–18°S). *J. South Am. Earth Sci.* 45, 6–23.
- Deer, W.A., Howie, R.A., Zussman, J., 1982. Rock-forming Minerals. In: Orthosilicates, vol. 1A. Longman, London.
- Dietz, V., 1973. Experiments on the influence of transport on shape and roundness of heavy minerals. *Contrib. Sediment.* 1, 103–125.
- Dunkl, I., Székely, B., 2002. Component analysis with visualization of fitting – PopShare, a windows program for data analysis. – goldschmidt conference abstracts 2002. *Geochim. Cosmochim. Acta* 66 (15A), 201.
- Dunkl, I., Frisch, W., Kuhlemann, J., Brügel, A., 2009. Pebble population dating as an additional tool for provenance studies - examples from the Eastern Alps. *Geol. Soc. Lond. Spec. Publ.* 324, 125–140.
- Franz, G., Spear, F.S., 1985. Aluminous titanite sphene from the eclogite zone, South-central Tauern Window, Austria. *Chem. Geol.* 50, 33–46.
- Frei, D., Gerdes, A., 2009. Precise and accurate *in situ* U-Pb dating of zircon with high sample throughput by automated LA-SF-ICP-MS. *Chem. Geol.* 261, 261–270.
- Freise, F.W., 1931. Untersuchung von Mineralen auf Abnutzbarkeit bei Verfrachtung im Wasser. *Tschermaks Mineral. Petrogr. Mitt.* 41, 1–7.
- Frost, B.R., Chamberlain, K.R., Schumacher, J.C., 2000. Spheine (titanite): phase relations and role as a geochronometer. *Chem. Geol.* 172, 131–148.
- García, W., 1968. Geología de los cuadrángulos de Mollendo (34-r) y La Joya (34-s), vol. 19. Boletín del Servicio de Geología y Minería, Lima, Perú, p. 93.
- Garzione, C.N., Hoke, G.D., Libarkin, J.C., Withers, S., MacFadden, B., Eiler, J., Ghosh, P., Mulch, A., 2008. Rise of the Andes. *Science* 320 (5881), 1304–1307.
- Gawthorpe, R.L., Colella, A., 1990. Tectonic controls on coarse-grained delta depositional systems in rift basins. *Spec. Publs. Int. Ass. Sediment.* 10, 113–127.
- Gawthorpe, R.L., Hurst, J.M., Sladen, C.P., 1990. Evolution of Miocene footwall-derived fan deltas, Gulf of Suez, Egypt: implications for explorations. *Bull. Am. Assoc. Petrol. Geol. Bull.* 74, 1077–1086.
- Gehrels, G.E., Valencia, V.A., Ruiz, J., 2008. Enhanced precision, accuracy, efficiency, and spatial resolution of U-Pb ages by laser ablation-multicollector-inductively coupled plasma-mass spectrometry. *Geochem. Geophys. Geosystems* 9 (3), 13.
- Gilder, S., Rousse, S., Farber, D., Sempere, T., Torres, V., Palacios, O., 2003. Post-Middle Oligocene origin of paleomagnetic rotations in Upper Permian to Lower Jurassic rocks from northern and southern Peru. *Earth Planet. Sci. Lett.* 210, 233–248.
- Gregory-Wodzicki, K.M., 2000. Uplift history of the Central and Northern Andes: a review. *Geol. Soc. Am. Bull.* 112 (7), 1091–1105.
- Haq, B., Hardenbol, J., Vail, P., 1987. Chronology of fluctuating sea levels since the Triassic (250 million years ago to present). *Science* 235, 1156–1167.
- (Chapter 16) Haschke, M., Günther, A., Melnick, D., Echtler, H., Reutter, K.J., Scheuber, E., Oncken, O., 2006. Central and southern Andean tectonic evolution inferred from arc magmatism. In: Oncken, O., Chong, G., Franz, G., Giese, P., Götz, H.J., Ramos, V.A., Strecker, M.R., Wigger, P. (Eds.), *The Andes, Active Subduction Orogeny*. Springer-Verlag Berlin Heidelberg, Berlin, Germany, pp. 337–353.
- Hubert, J.F., 1962. A zircon-tourmaline-rutile maturity index and the interdependence of the composition of heavy mineral assemblages with the gross composition and texture of sandstones. *J. Sediment. Petrol.* 32, 440–450.
- Hutton, C.O., 1950. Studies of heavy detrital minerals. *Bull. Geol. Soc. Am.* 61, 635–710.
- Isacks, B.L., 1988. Uplift of the Central Andean plateau and bending of the Bolivian orocline. *J. Geophys. Res.* 93, 3211–3231.
- Jacay, J., Sempere, T., Husson, L., Pino, A., 2002. Structural characteristics of the incapuquio fault system, southern Peru. In: *V International Symposium on Andean Geodynamics ISAG, Extended Abstracts*. Toulouse, France, pp. 319–321.
- Jackson, S.E., Longerich, H.P., Dunning, G.R., Fryer, B.J., 1992. The application of laser ablation microprobe-inductively coupled plasma-mass spectrometry (LAM-ICP-MS) to *in-situ* trace element determinations in minerals. *Can. Mineral.* 30, 1049–1064.
- Jackson, S.E., Pearson, N.J., Griffin, W.L., Belousova, E.A., 2004. The application of laser ablation-inductively coupled plasma-mass spectrometry to *in situ* U-Pb zircon geochronology. *Chem. Geol.* 211, 47–69.
- Jenks, W.F., Harris, E.G., 1953. Plutonics near Arequipa as a petrologic sample of the coastal batholith of Peru. *Bol. la Soc. Geol. del Perú* 26, 79–94.
- Jordan, T.E., Isacks, B.L., Allmendinger, R.W., Brewer, J.A., Ramos, V.A., Ando, C.J., 1983. Andean tectonics related to geometry of subducted Nazca plate. *Geol. Soc. Am. Bull.* 94 (3), 341–361.
- Kay, S.M., Mpodozis, C., Coira, B., 1999. Magmatism, tectonism and mineral deposits of the Central Andes (22°–33°S latitude). In: Skinner, B.J. (Ed.), *Geology and Ore Deposits of the Central Andes*, vol. 7. Society of Economic Geology Special Publication, pp. 27–59.
- Kosler, J., Sylvester, P.J., 2007. Present Trends and the future of zircon in geochronology: laser ablation in ICPMS. *Rev. Mineral. Geochem.* 53 (1), 243–275.
- Kosler, J., Fonneland, H., Sylvester, P., Tubrett, M., Pedersen, R.B., 2002. U-Pb dating of detrital zircons for sediment provenance studies- a comparison of laser ablation ICPMS and SIMS techniques. *Chem. Geol.* 182, 605–618.
- Laetsch, T., Downs, R.T., 2006. Software for identification and refinement of cell parameters from powder diffraction data of minerals using the RRUFF project and american mineralogist Crystal structure Databases. In: *19th General Meeting of the International Mineralogical Association*, Kobe, Japan, 2006, 23–28.
- Loewy, S.L., Connelly, J.N., Dalziel, I., 2004. An orphaned basement block: the Arequipa-Antofalla basement of the central Andean margin of South America. *Geol. Soc. Am. Bull.* 116, 171–187.
- Ludwig, K.R., 2003. User's Manual for Isoplot 3.00: a Geochronological Toolkit for Microsoft Excel: Berkeley Geochronology, vol. 4. Center Special Publication, p. 70.
- Machář, J., Sébrier, M., Huamán, D., Mercier, J.L., 1986. Tectónica Cenozoica de la Margen Continental Peruana. *Bol. la Soc. Geol. del Perú* 76, 45–77.
- Mahlburg-Kay, S., Godoy, E., Kurtz, A., 2005. Episodic arc migration, crustal thickening, subduction erosion, and magmatism in the south-central Andes. *Geol. Soc. Am. Bull.* 117 (1–2), 67–88.
- Mamani, M., Wörner, G., Sempere, T., 2010. Geochemical variations in igneous rocks of the Central Andean orocline (13°S to 18°S): tracing crustal thickening and magma generation through time and space. *Geol. Soc. Am.* 122, 162–182.
- Mamani, M., Rodríguez, R., Acosta, H., Jaimes, F., Navarro, P., Carlotto, V., 2012. Características Litológicas y Geoquímicas más Resaltantes de los Arcos Magnéticos del Perú desde el Ordovícico. In: *XVI Congreso Peruano de Geología*, Lima. Sociedad Geológica del Perú, Resúmenes Extendidos, p. 5.
- Mange, M.A., Maurer, H.F.W., 1992. Heavy Minerals in Colour. Hong Kong. Chapman & Hall, London.
- Marocco, R., Noblet, C., 1990. Sedimentation, tectonism and volcanism relationships in two Andean basins of southern Peru. *Geol. Rundsch.* 79 (1), 111–120.
- Marocco, R., Delfaud, J., Lavenu, A., 1985. Ambiente deposicional de una cuenca continental intramontañosa andina: el Grupo Moquegua (sur de Perú) primeros resultados. *Soc. Geol. del Perú* 75, 73–90.
- Martignole, J., Martelat, J.E., 2003. Regional-scale Grenvillian-age UHT metamorphic in the Mollendo-Camana block (basement of the Peruvian Andes). *J. Metamorph. Geol.* 21, 99–120.
- Martínez, W., Cervantes, J., 2003. Rocas Igneas en el Sur del Perú. Nuevos Datos Geocronológicos, Geoquímicos y Estructurales entre los paralelos 16° y 18°30' Latitud Sur. INGEMMET, Lima, Perú. Estudios Regionales, Boletín No. 26, Serie D, p. 146.
- Martinod, J., Espurt, N., Guillaume, B., Husson, L., Roperch, P., 2010. Horizontal subduction zones, convergence velocity and the building of the Andes. *Earth Planet. Sci. Lett.* 299, 299–309.
- Moreno, C., Horton, B., Caballero, V., Mora, A., Parra, M., Sierra, J., 2011. Depositional and provenance record of the Paleogene transition from foreland to hinterland basin evolution during Andean orogeny, northern Middle Magdalena Valley Basin, Colombia. *J. South Am. Earth Sci.* 31, 246–263.
- Morton, A.C., 1991. Geochemical studies of detrital heavy minerals and their application to provenance research. *Geol. Soc. Lond. Spec. Publ.* 57 (1), 31.
- Morton, A.C., Hallsworth, C., 1994. Identifying provenance-specific features of detrital heavy mineral assemblages in sandstones. *Sediment. Geol.* 90, 241–256.
- Morton, A.C., Hallsworth, C.R., 1999. Processes controlling the composition of heavy mineral assemblages in sandstones. *Sediment. Geol.* 124, 3–29.
- Mukasa, S.B., 1986. Zircon U-Pb ages of super-units in the Coastal Batholith, Peru: implications for magmatic and tectonic processes. *Geol. Soc. Am. Bull.* 97 (2), 241–254.
- Mukasa, S.B., Henry, D.J., 1990. The San Nicolás batholith of coastal Peru: early Paleozoic continental arc or continental rift magmatism? *J. Geol. Soc.* 147, 27–39.
- (Chapter 1) Oncken, O., Hindle, D., Kley, J., Elger, K., Victor, P., Schemmann, K., 2006. Deformation of the Central Andean upper plate system—Facts, Fiction, and constraints for the plateau models. In: Oncken, O., Chong, G., Franz, G., Giese, P., Götz, H.J., Ramos, V.A., Strecker, M.R., Wigger, P. (Eds.), *The Andes, Active Subduction Orogeny*. Springer-Verlag Berlin Heidelberg, Berlin, Germany, pp. 1–27.
- Palacios, O., Chacón, N., 1989. Evolución geomorfológica del territorio Peruano. Sociedad Geográfica de Lima, p. 12.
- Palacios, O., Klinck, B.A., De La Cruz, J., Allison, R.A., De La Cruz, N., Hawkins, M.P., 1993. Geología de la Cordillera Occidental y Altiplano al oeste del Lago Titicaca–Sur del Perú. Instituto Geológico Minero y Metalúrgico (INGEMMET), Lima, Perú. Boletín No. 42.
- Pardo-Casas, F., Molnar, P., 1987. Relative motion of the Nazca (Farallon) and South American plates since Late Cretaceous time. *Tectonics* 6 (3), 233–248.
- Pecho, V., Morales, G., 1969. Geología de los Cuadrángulos de Camaná y La Yesera. Boletín No. 21, Serie (A). Boletín de la Carta Geológica Nacional (INGEMMET), Lima, Perú, p. 72.

- PERUPETRO, 2003. Peruvian Petroleum, a Renewed Exploration Opportunity. Lima, Perú. Report of PERUPETRO, p. 159.
- Pitcher, W.S., Atherton, M.P., Cobbing, E.J., Beckinsale, R.D., 1985. Magmatism at a Plate Edge: the Peruvian Andes. Glasgow, Blackie & Son, and New York, Halsted Press, p. 328.
- Quang, C., Clark, A., Lee, J.K., Hawkes, N., 2005. Response of supergene processes to episodic Cenozoic uplift, pediment erosion, and ignimbrite eruption in the porphyry copper province of southern Peru. *Econ. Geol.* 100 (1), 87–110.
- Rivera, R., 1950. Geología del Valle de Camaná y Majes. Tesis de Grado. Universidad Nacional San Agustín, Arequipa.
- Roperch, P., Sempere, T., Macedo, O., Arriagada, C., Fornari, M., Tapia, C., García, M., Laj, C., 2006. Counterclockwise rotation of late Eocene–Oligocene fore-arc deposits in southern Peru and its significance for oroclinial bending in the central Andes. *Tectonics* 25 (3), 29.
- Rüegg, W., 1952. The Camaná Formation and its bearing on the Andean post-orogenic uplift. *Bull. Assoc. Suisse Geol. Ing. Petrol.* 19, 7–12.
- Salas, O.R., René, F.R., Montesinos, F., 1966. Geología y recursos minerales del departamento de Arica: Provincia de Tarapacá. Instituto de Investigaciones Geológicas.
- Schildgen, T.F., Hodges, K.V., Whipple, K.X., Reiners, P.W., Pringle, M.S., 2007. Uplift of the western margin of the Andean plateau revealed from canyon incision history, southern Peru. *Geology* 35 (6), 523–526.
- Schildgen, T., Hodges, K., Whipple, K., Pringle, M., van Soest, M., Cornell, K., 2009. Late Cenozoic structural and tectonic development of the western margin of the central Andean Plateau in southwest Peru. *Tectonics* 28, 21.
- Schlunegger, F., Matter, A., Burbank, D.W., Leu, W., Mange, M., Matyas, J., 1997. Sedimentary sequences, seismofacies and evolution of depositional systems of the Oligo/Miocene Lower Freshwater Molasse Group, Switzerland. *Basin Res.* 9, 1–26.
- Scott, D.J., St Onge, M.R., 1995. Constraints on Pb closure temperature in titanite based on rocks from the Ungava Orogen, Canada: implications for U-Pb geochronology and P-T-t path determinations. *Geology* 23, 1123–1126.
- Sempere, T., Fornari, M., Acosta, J., Flores, A., Jacay, J., Peña, D., Roperch, P., Taipe, E., 2004. Estratigrafía, geocronología y paleotectónica de los depósitos de antearco del sur del Perú. In: XII Congreso Peruano de Geología, Lima. Sociedad Geológica del Perú, Resúmenes Extendidos, pp. 533–536.
- Shackleton, R.M., Ries, A.C., Coward, M.P., Cobbold, P.R., 1979. Structure, metamorphism and geochronology of the Arequipa Massif of coastal Peru. *J. Geol. Soc. Lond.* 136 (2), 195–214.
- Sirccombe, K.N., 2004. AgeDisplay: an EXCEL workbook to evaluate and display univariate geochronological data using binned frequency histograms and probability density distributions. *Comput. Geosciences* 30, 21–31.
- Sláma, J., Kosler, J., Condon, D.J., Crowley, J.L., Gerdes, A., Hanchar, J.M., Horstwood, M.S.A., Morris, G.A., Nasdala, L., Norberg, N., Schaltegger, U., Schoene, B., Tubrett, M.N., Whitehouse, M.J., 2008. Plesovice zircon – a new natural reference material for U-Pb and Hf isotopic microanalysis. *Chem. Geol.* 249, 1–35.
- Sobolev, S.V., Babeyko, A.Y., 2005. What drives orogeny in the Andes? *Geol. Soc. Am. Bull.* 33 (8), 617–620.
- Somoza, R., 1998. Updated azca (Farallon)–South America relative motions during the last 40 My: implications for mountain building in the central Andean region. *J. South Am. Earth Sci.* 11 (3), 211–215.
- Sun, J., Yang, J., Wu, F., Xie, L., Yang, Y., Liu, Z., Li, X., 2012. *In situ* U-Pb dating of titanite by LA-ICPMS. *Chin. Sci. Bull.* 57 (20), 2506–2516.
- Thiel, G.A., 1940. The relative resistance to abrasion of mineral grains of sand size. *J. Sediment. Petrol.* 10, 103–124.
- Thouret, J.C., Wörner, G., Finizola, A., Legeley-Padovani, A., 2002. Valley evolution, uplift, volcanism, and related hazards in the central Andes of Southern Peru. In: 5th International Symposium on Andean Geodynamics. ISAG. Toulouse, France, pp. 641–644.
- Thouret, J.C., Wörner, G., Gunnell, Y., Singer, B., Zhang, X., Souriot, T., 2007. Geochronologic and stratigraphic constraints on canyon incision and Miocene uplift of the Central Andes in Peru. *Earth Planet. Sci. Lett.* 263, 151–166.
- Tosdal, R.M., Farrar, E., Clark, A., 1981. K-Ar geochronology of the late cenozoic volcanic rocks of the Cordillera occidental, Southernmost Peru. *J. Volcanol. Geotherm. Res.* 10, 157–173.
- Vargas, L., 1970. Geología del Cuadrángulo de Arequipa, vol. 24. Dirección de Geología Regional, p. 64. INGEMMET. Lima, Perú, Boletín.
- Vermeesch, P., 2004. How many grains are needed for a provenance study? *Earth Planet. Sci. Lett.* 224, 441–451.
- Vermeesch, P., 2012. On the visualisation of detrital age distributions. *Chem. Geol.* 312–313.
- Vicente, J.C., 1989. Early late Cretaceous overthrusting in the western cordillera of southern Peru. In: Erickson, G.E., Canas-Pinochet, M.T., Reinemund, J.A. (Eds.), *Geology of the Andes and its Relation to Hydrocarbon and Mineral Resources*, Circum-Pacific Council for Energy and Mineral Resources Earth Science Series, vol. 11, pp. 91–117.
- von Eynatten, H., Dunkl, I., 2012. Assessing the sediment factory: the role of single grain analysis. *Earth Sci. Rev.* 115, 97–120.
- von Eynatten, H., Voigt, T., Meier, A., Franzke, H.J., Gaupp, R., 2008. Provenance of Cretaceous clastics in the Subhercynian Basin: constraints to exhumation of the Harz Mountains and timing of inversion tectonics in Central Europe. *Int. J. Earth Sci.* 97, 1315–1330.
- Weltje, G.J., von Eynatten, H., 2004. Quantitative provenance analysis of sediments: review and outlook. *Sediment. Geol.* 171, 1–11.
- Whitney, D.L., Evans, B.W., 2010. Abbreviations for names of rock-forming minerals. *Am. Mineral.* 95, 185–187.
- Wiedenbeck, M., Allé, P., Corfu, F., Griffin, W.L., Meier, M., Oberli, F., von Quadt, A., Roddick, J.C., Spiegel, W., 1995. Three natural zircon standards for U-Th–Pb, Lu–Hf, trace element and REE analyses. *Geostand. Newslett.* 19, 1–23.
- Wilson, J., García, W., 1962. Geología de los Cuadrángulos de Pachía y Palca, vol. 2 (4). Comisión de la Carta Geológica Nacional, Lima, Perú, p. 81.
- Wipf, M., 2006. Evolution of the Western Cordillera and Coastal Margin of Peru: Evidence from Low-temperature Thermochronology and Geomorphology (PhD thesis). Swiss Federal Institute of Technology Zürich. Swiss Federal Institute of Technology, p. 163.
- Wörner, G., Uhlig, D., Kohler, I., Seyfried, H., 2002. Evolution of the West Andean Escarpment at 18°S (N. Chile) during the last 25 Ma: uplift, erosion and collapse through time. *Tectonophysics* 345, 183–198.
- Wotzlaw, J., Decou, A., von Eynatten, H., Wörner, G., Frei, D., 2011. Jurassic to Paleogene tectono-magmatic evolution of northern Chile and adjacent Bolivia from detrital zircon U-Pb geochronology and heavy mineral provenance. *Terra Nova* 23, 399–406.